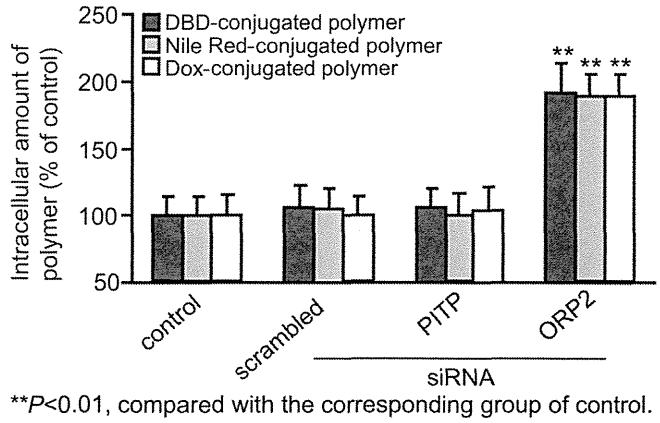

Fig. 6. Effect of siRNA-induced knockdown of ORP2 and PITP on the intracellular amounts of polymers. The figure shows the intracellular amounts of polymer under suppressing conditions for ORP2 or PITP at 24 h after the addition of micelles to HeLa cells. $^{**}P < 0.01$ compared with the corresponding control group. Each value represents the mean ± SD ($n = 6$).

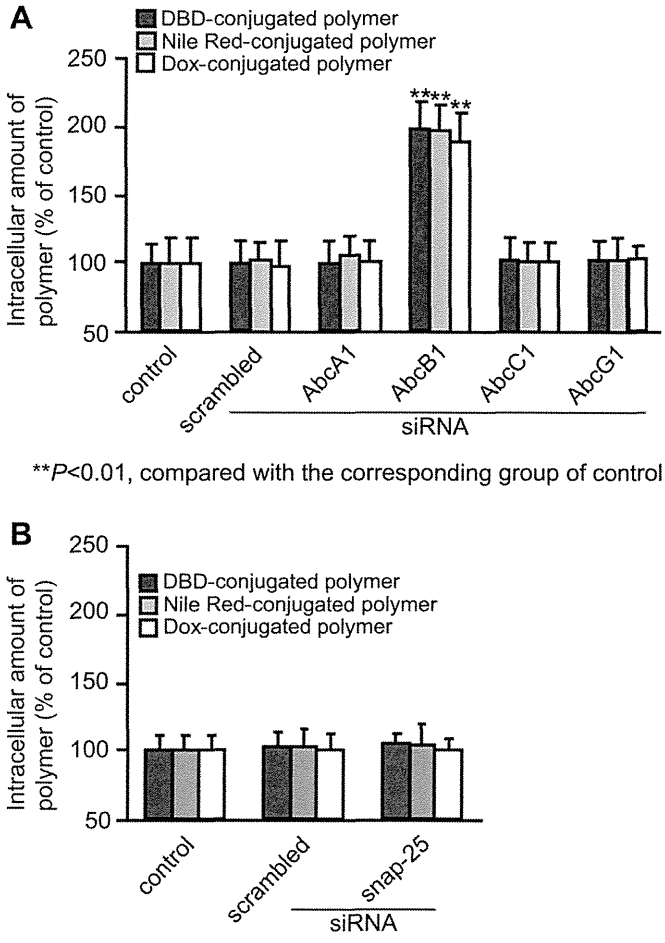

Fig. 7. (A) Effect of siRNA-induced knockdown of ABC transporters on the intracellular amounts of polymers. The figure shows the intracellular amounts of polymer under suppressing conditions for various ABC transporters (ABCA1, ABCB1, ABCC1, and ABCG1) at 24 h after the addition of micelles to HeLa cells. (B) The intracellular amounts of polymers under suppressing conditions for snap-25 at 24 h after the addition of micelles to HeLa cells. The cells were transfected with siRNAs against the targeted proteins by using Lipofectamine RNAiMAX according to the recommended protocols. $^{**}P < 0.01$ compared with the corresponding control group. Each value represents the mean ± SD ($n = 6$).

from endosomes or lysosomes to the ER (Fig. 5C). Our results also suggest that ER-to-Golgi transport is not involved in the intracellular trafficking of block copolymers (Supplementary Fig. 4). This is consistent with our observation that the polymer did not localize to the Golgi apparatus (Fig. 4B). Taken with the results of the FRET micelle experiments, the confocal images suggest that the micelles used in this study dissociate into their individual components in late endosomes, and after dissociation, the polymers are extracted by NPC1 from the endosomes and transferred to the ER (Fig. 9). We confirmed that 4-phenyl-1-butanol, which was conjugated to the polymers to increase their hydrophobicity, was not released from the polymers under the experimental conditions used (Supplementary Fig. 6). Therefore, the release of the conjugated compounds is not the driving force for the dissociation of the micelles in late endosomes or lysosomes. The driving force for this dissociation remains to be elucidated.

NPC1 facilitates the trafficking of low density lipoprotein-derived cholesterol from the late endosome to various destinations such as the plasma membrane, the trans-golgi network, and the ER [39]. Similarly, it appears that NPC1 enhances the trafficking of dissociated polymers from late endosomes to the ER. Although direct trafficking from the late endosome to the plasma membrane is a possibility [40], such trafficking would probably represent a small proportion of the total trafficking given our finding that the inhibition of trafficking from the ER to the plasma membrane led to the retention of most of the intracellular block copolymers. Sahay G et al. reported that NCP1 is an important regulator of the major recycling pathways of lipid nanoparticle-delivered siRNA, although they did not investigate the trafficking of the carrier components, but rather tracked the labeled siRNA. They demonstrated that NPC1-deficient cells show enhanced cellular retention of lipid nanoparticles inside late endosomes because of the decrease in motility of late endosomes [40,41]. These findings indicate that NPC1 is a key factor in determining the fate of block copolymers.

Although some of the block copolymers might have been retained in vesicles and transferred to lysosomes, the dissociated polymers in the late endosomes were transported to the ER. Our results also indicate that encapsulated drugs could be released from these micellar carriers in late endosomes and diffuse into the cytoplasm at this stage, demonstrating that such micelles are suitable for the intracellular delivery of degradable compounds, such as nucleic acids or proteins, and can minimize the degradation of these compounds in lysosomes. We also investigated the extracellular efflux mechanisms of block copolymers. As shown in Fig. 6, the transport of block copolymers to the cell membrane was affected by ORP2 (Fig. 9). ORP2 is involved in the vesicle-independent intermembrane transport of lipophilic compounds [32–34], and the ER possesses closed sites at the cell membrane [42]. Hao et al. reported that endogenous cholesterol is transported to cell membranes via the ER [43]. Therefore, the block copolymers in the present study might also be transferred to the cell membrane via these closed sites (Fig. 9). Following the transfer to the plasma membrane, efflux of the block copolymers mainly occurred via ABCB1 but not ABCA1, ABCC1, or ABCG1 (Figs. 7 and 9). SNARE proteins, such as snap-25, control the extracellular efflux of various compounds, including proteins and lipids, via exocytosis [44,45]. Although the expression levels of SNARE-related proteins are high in specific cancer cells, including HeLa cells [44–46], exocytosis did not appear to be involved in the extracellular efflux of block copolymers from HeLa cells (Fig. 7B), and the block copolymers used in our studies were effluxed only through the ABCB1.

Lastly, we investigated the molecular mechanism of block copolymer efflux through transporters by using vesicles that expressed ABCB1. All of the polymers, regardless of PEG chain length, polymerization degree of P(Asp), or fluorescent compound,

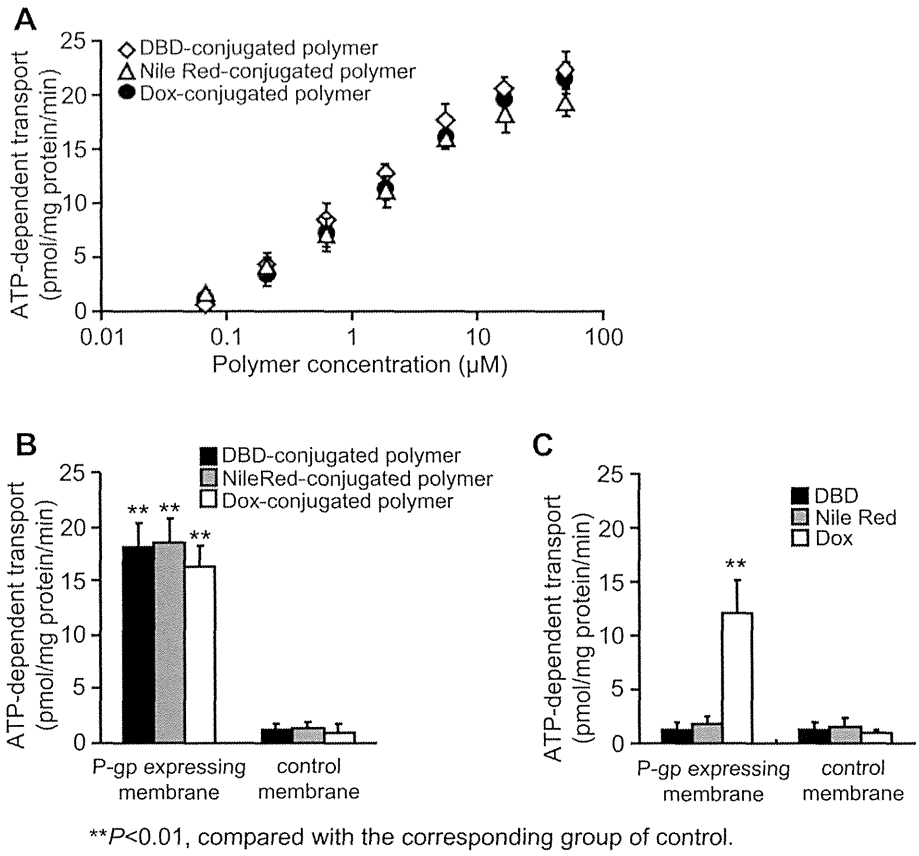

Fig. 8. ATP-dependent uptake of polymers by ABCB1-expressing membrane vesicles. Suspensions of membranes expressing ABCB1, or control membranes that did not express ABCB1 (50 μL each) were plated on a 96-well plate. (A) Increasing polymer transport with increasing polymer concentration. Samples at the indicated concentration were added to each well, respectively, and the plates were incubated at 37 °C for 5 min. After washing by centrifugation, the fluorescence intensity of the transported polymers was measured. Each value represents the mean ± SD ($n = 6$). (B) Transport of fluorescent polymers into vesicles expressing ABCB1. $^{**}P < 0.01$, compared with the corresponding control group. Each value represents the mean ± SD ($n = 6$). (C) Transport of free fluorescent compounds into vesicles expressing ABCB1. $^{**}P < 0.01$, compared with the corresponding control group. Each value represents the mean ± SD ($n = 6$).

underwent similar transport into the vesicles expressing ABCB1 (Fig. 8B). Free DBD and Nile Red were not, however, transported through ABCB1 (Fig. 8C), indicating that the observed changes in fluorescence did in fact correspond to the transport of the polymers and not to that of dissociated Dox, DBD, or Nile Red. This result indicates that the block copolymers themselves are crucial to their transport by ABCB1, and that the conjugated fluorescent compound is not recognized by ABCB1. The ABCB1 transporter plays a critical role in drug clearance, including urinary excretion in the kidneys, and biliary excretion in the liver [47]. We are currently investigating the role of the ABCB1 transporter in the dynamics and clearance of the polymer and encapsulated drugs *in vivo*.

All of the micelles used in this study showed the same intracellular trafficking and the same proteins were involved in that trafficking, independent of PEG chain length, polymerization degree of P(Asp), and the hydrophobic moiety introduced into the core segment within the range investigated. To determine whether the intracellular trafficking and the molecular mechanism were specific to the block copolymer we used, we tested the more hydrophilic polymer dextran. Dextran is a macropinocytosis marker, and in fact its internalization was inhibited by the macropinocytosis inhibitor EIPA (Supplementary Fig. 7). Because it is possible that macropinosomes directly fuse with NPC1-positive late endosomes [48], dextran can be recycled to the extracellular milieu by NPC1. However, NPC1 was not involved in the trafficking of dextran from the late endosome (Supplementary Fig. 3). Moreover, knockdown of ORP2 and ABCB1 expression, which is involved in block copolymer trafficking, was not involved in the intracellular trafficking of dextran (Supplementary Fig. 5). We also tested a hydrophobic nanoparticle (a polystyrene nanoparticle) and a hydrophilic nanoparticle (a silica nanoparticle) with respect to their intracellular trafficking. The internalization of these nanoparticles was mediated by both clathrin-mediated endocytosis and caveolae-mediated endocytosis (Supplementary Fig. 7) similarly to the block copolymers and micelles we used. However, NPC1, ORP2, and ABCB1 were not involved in the intracellular trafficking of these nanoparticles (Supplementary Figs. 3 and 5). Yet, the efflux of dextran, polystyrene nanoparticles, and silica nanoparticles is controlled by the exocytosis protein snap-25 (Supplementary Fig. 8). Thus, the findings described in this report regarding the intracellular fate of the block copolymers and the intrinsic proteins involved in their trafficking are specific to these block copolymers. From a safety standpoint, further studies are needed to elucidate the physicochemical properties of block copolymers that determine their intracellular trafficking and fate so that we might be able to predict the potential for accumulation of newly developed block copolymers inside cells and/or their efflux from cells. It will also be necessary to elucidate the intracellular trafficking and fate of block copolymers in different cell types.

5. Conclusions

We have characterized here the intracellular trafficking and fate of different block copolymer micelles and their dissociated polymers, from intracellular uptake to extracellular efflux. In addition, we identified three proteins that are involved in the intracellular

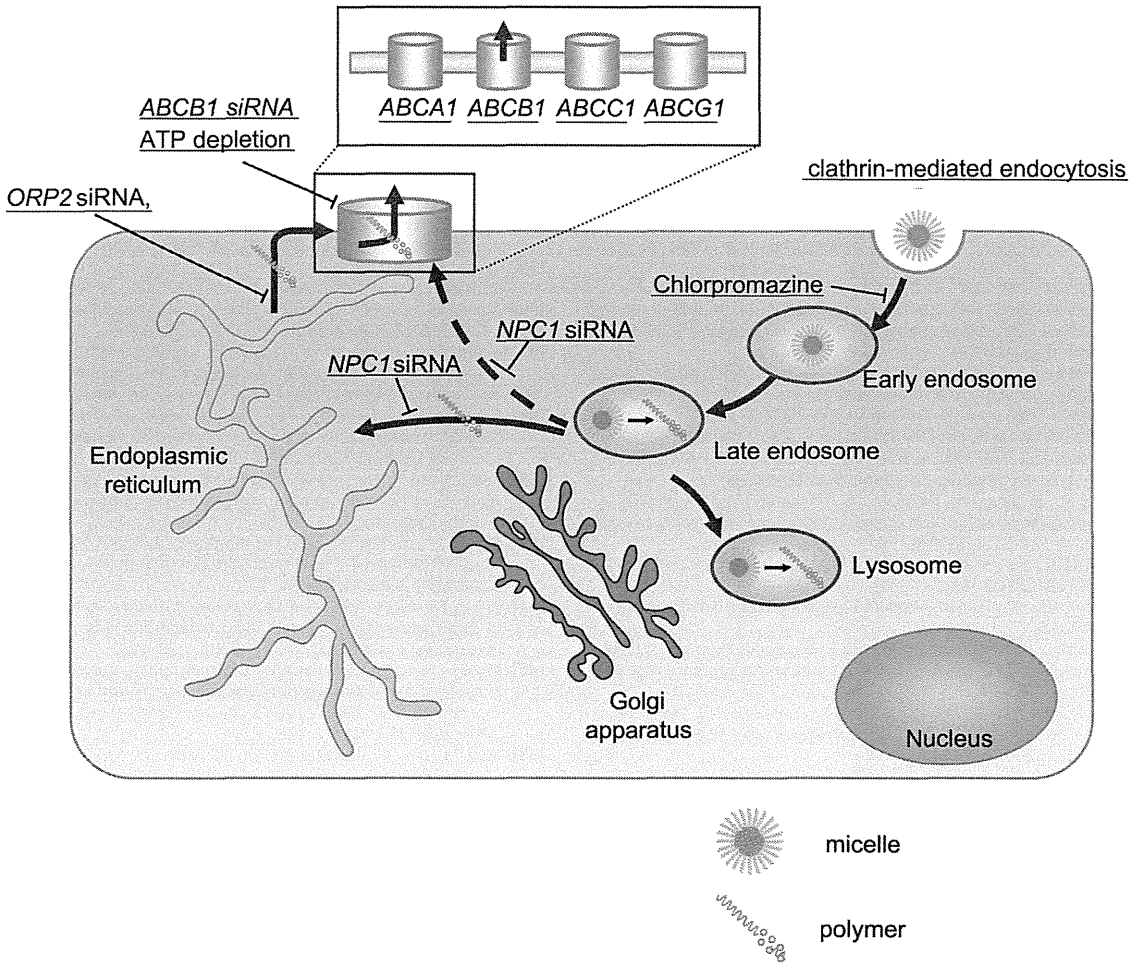

Fig. 9. Predicted mechanism of intracellular trafficking of micelles and polymers used in this study.

trafficking of these polymers: NPC1, ORP2, and ABCB1 (Fig. 9). By using FRET micelles, we showed that the dissociation of the micelles occurs mainly in late endosomes and that NPC1 seems to have a key role in the dissociation of micelles and in the intermembrane transfer of the block copolymers.

Exocytosis is well-known efflux route for nanoparticles internalized by endocytosis. Our study has elucidated a unique trafficking and efflux route for the components of block copolymer micelles in which NPC1 and ORP2 play essential role in the transfer of the block copolymers to their efflux via the transporter ABCB1. This route can prevent the accumulation of components inside the cells after intracellular uptake via endocytosis. Such knowledge may help improve the therapeutic efficacy and minimize the safety risks of block copolymer micelles.

Acknowledgments

This work was supported in part by Public-Private Sector Joint Research on Publicly Essential Drugs from the Japan Health Sciences Foundation, by Health and Labour Sciences Research Grants from the Ministry of Health, Labour and Welfare of Japan, and by JSPS KAKENHI Grant number 24590070. We thank Nippon Kayaku Co. Ltd for providing the block copolymers.

Appendix A. Supplementary data

Supplementary data related to this article can be found at http://dx.doi.org/10.1016/j.biomaterials.2013.11.027.

References

[1] Barenholz Y. Doxil® – the first FDA-approved nano-drug: lessons learned. J Control Release 2012;160:117–34.
[2] Duncan R, Gaspar R. Nanomedicine(s) under the microscope. Mol Pharm 2011;8:2101–41.
[3] Ferrari M. Cancer nanotechnology: opportunities and challenges. Nat Rev Cancer 2005;5:161–71.
[4] Kataoka K, Kwon GS, Yokoyama M, Okano T, Sakurai Y. Block copolymer micelles as vehicles for drug delivery. J Control Release 1993;24:119–32.
[5] Nishiyama N, Kataoka K. Current state, achievements, and future prospects of polymeric micelles as nanocarriers for drug and gene delivery. Pharmacol Ther 2006;112:630–48.
[6] Torchilin VP. PEG-based micelles as carriers of contrast agents for different imaging modalities. Adv Drug Deliv Rev 2002;54:235–52.
[7] Kabanov A, Zhu J, Alakhov V. Pluronic block copolymers for gene delivery. Adv Genet 2005;53:231–61.
[8] Uchino H, Matsumura Y, Negishi T, Koizumi F, Hayashi T, Honda T, et al. Cisplatin-incorporating polymeric micelles (NC-6004) can reduce nephrotoxicity and neurotoxicity of cisplatin in rats. Br J Cancer 2005;93:678–87.
[9] Hamaguchi T, Matsumura Y, Suzuki M, Shimizu K, Goda R, Nakamura I, et al. NK105, a paclitaxel-incorporating micellar nanoparticle formulation, can extend in vivo antitumour activity and reduce the neurotoxicity of paclitaxel. Br J Cancer 2005;92:1240–6.
[10] Koizumi F, Kitagawa M, Negishi T, Onda T, Matsumoto S, Hamaguchi T, et al. Novel SN-38-incorporating polymeric micelles, NK012, eradicate vascular endothelial growth factor-secreting bulky tumors. Cancer Res 2006;15(66):10048–56.
[11] Murakami M, Cabral H, Matsumoto Y, Wu S, Kano MR, Yamori T, et al. Improving drug potency and efficacy by nanocarrier-mediated subcellular targeting. Sci Transl Med 2011;3:64ra2.
[12] Sahay G, Batrakova EV, Kabanov AV. Different internalization pathways of polymeric micelles and unimers and their effects on vesicular transport. Bioconjug Chem 2008;19:2023–9.
[13] Hatakeyama H, Akita H, Harashima H. A multifunctional envelope type nano device (MEND) for gene delivery to tumours based on the EPR effect:

a strategy for overcoming the PEG dilemma. Adv Drug Deliv Rev 2011;63:152–60.
[14] Sakai-Kato K, Ishikura K, Oshima Y, Tada M, Suzuki T, Ishii-Watabe A, et al. Evaluation of intracellular trafficking and clearance from HeLa cells of doxorubicin-bound block copolymers. Int J Pharm 2012;423:401–9.
[15] Nakanishi T, Fukushima S, Okamoto K, Suzuki M, Matsumura Y, Yokoyama M, et al. Development of the polymer micelle carrier system for doxorubicin. J Control Release 2001;74:295–302.
[16] Rejman J, Bragonzi A, Conese M. Role of clathrin- and caveolae-mediated endocytosis in gene transfer mediated by lipo- and polyplexes. Mol Ther 2005;12:468–74.
[17] Perez AP, Cosaka ML, Romero EL, Morilla MJ. Uptake and intracellular traffic of siRNA dendriplexes in glioblastoma cells and macrophages. Int J Nanomed 2011;6:2715–28.
[18] Tomás M, Martínez-Alonso E, Ballesta J, Martínez-Menárguez JA. Regulation of ER-Golgi intermediate compartment tubulation and mobility by COPI coats, motor proteins and microtubules. Traffic 2010;11:616–25.
[19] Uematsu K, Seki N, Seto T, Isoe C, Tsukamoto H, Mikami I, et al. Targeting the Wnt signaling pathway with dishevelled and cisplatin synergistically suppresses mesothelioma cell growth. Anticancer Res 2007;27:4239–42.
[20] Chen H, Kim S, He W, Wang H, Low PS, Park K, et al. Fast release of lipophilic agents from circulating PEG-PDLLA micelles revealed by in vivo forster resonance energy transfer imaging. Langmuir 2008;24:5213–7.
[21] Miller T, Rachel R, Besheer A, Uezguen S, Weigandt M, Goepferich A. Comparative investigations on in vitro serum stability of polymeric micelle formulations. Pharm Res 2012;29:448–59.
[22] Ioannou YA. Multidrug permeases and subcellular cholesterol transport. Nat Rev Mol Cell Biol 2001;2:657–68.
[23] Mineo C, Anderson RG. Potocytosis. Robert Feulgen Lecture. Histochem Cell Biol 2001;116:109–18.
[24] Hölttä-Vuori M, Alpy F, Tanhuanpää K, Jokitalo E, Mutka AL, Ikonen E. MLN64 is involved in actin-mediated dynamics of late endocytic organelles. Mol Biol Cell 2005;16:3873–86.
[25] Xu Y, Liu Y, Ridgway ND, McMaster CR. Novel members of the human oxysterol-binding protein family bind phospholipids and regulate vesicle transport. J Biol Chem 2001;276:18407–14.
[26] Ikonen E. Cellular cholesterol trafficking and compartmentalization. Nat Rev Mol Cell Biol 2008;9:125–38.
[27] Koivusalo M, Jansen M, Somerharju P, Ikonen E. Endocytic trafficking of sphingomyelin depends on its acyl chain length. Mol Biol Cell 2007;18:5113–23.
[28] Hanada K, Kumagai K, Yasuda S, Miura Y, Kawano M, Fukasawa M, et al. Molecular machinery for non-vesicular trafficking of ceramide. Nature 2003;426:803–9.
[29] Hanada K, Kumagai K, Tomishige N, Yamaji T. CERT-mediated trafficking of ceramide. Biochim Biophys Acta 2009;1791:684–91.
[30] Sato K, Nakano A. Mechanisms of COPII vesicle formation and protein sorting. FEBS Lett 2007;581:2076–82.
[31] Townley AK, Feng Y, Schmidt K, Carter DA, Porter R, Verkade P, et al. Efficient coupling of Sec23-Sec24 to Sec13-Sec31 drives COPII-dependent collagen secretion and is essential for normal craniofacial development. J Cell Sci 2008;121:3025–34.
[32] Laitinen S, Lehto M, Lehtonen S, Hyvärinen K, Heino S, Lehtonen E, et al. ORP2, a homolog of oxysterol binding protein, regulates cellular cholesterol metabolism. J Lipid Res 2002;43:245–55.
[33] Hynynen R, Laitinen S, Käkelä R, Tanhuanpää K, Lusa S, Ehnholm C, et al. Overexpression of OSBP-related protein 2 (ORP2) induces changes in cellular cholesterol metabolism and enhances endocytosis. Biochem J 2005;390:273–83.
[34] Hynynen R, Suchanek M, Spandl J, Bäck N, Thiele C, Olkkonen VM. OSBP-related protein 2 is a sterol receptor on lipid droplets that regulates the metabolism of neutral lipids. J Lipid Res 2009;50:1305–15.
[35] Wirtz KW. Phospholipid transfer proteins revisited. Biochem J 1997;324:353–60.
[36] Hsuan J, Cockcroft S. The PITP family of phosphatidylinositol transfer proteins. Genome Biol 2001;2: reviews 3011.1–3011.8.
[37] Ségui B, Allen-Baume V, Cockcroft S. Phosphatidylinositol transfer protein beta displays minimal sphingomyelin transfer activity and is not required for biosynthesis and trafficking of sphingomyelin. Biochem J 2002;366:23–34.
[38] Batrakova EV, Kabanov AV. Pluronic block copolymers: evolution of drug delivery concept from inert nanocarriers to biological response modifiers. J Control Release 2008;130:98–106.
[39] Sugii S, Lin S, Ohgami N, Ohashi M, Chang CC, Chang TY. Roles of endogenously synthesized sterols in the endocytic pathway. J Biol Chem 2006;281:23191–206.
[40] Sahay G, Querbes W, Alabi C, Eltoukhy A, Sarkar S, Zurenko C, et al. Efficiency of siRNA delivery by lipid nanoparticles is limited by endocytic recycling. Nat Biotechnol 2013;31:653–8.
[41] Zhang M, Dwyer NK, Love DC, Cooney A, Comly M, Neufeld E, et al. Cessation of rapid late endosomal tubulovesicular trafficking in Niemann-Pick type C1 disease. Proc Natl Acad Sci U S A 2001;98:4466–71.
[42] Pichler H, Gaigg B, Hrastnik C, Achleitner G, Kohlwein SD, Zellnig G, et al. A subfraction of the yeast endoplasmic reticulum associates with the plasma membrane and has a high capacity to synthesize lipids. Eur J Biochem 2001;268:2351–61.
[43] Hao M, Lin SX, Karylowski OJ, Wüstner D, McGraw TE, Maxfield FR. Vesicular and non-vesicular sterol transport in living cells. The endocytic recycling compartment is a major sterol storage organelle. J Biol Chem 2002;277:609–17.
[44] Némoz-Gaillard E, Bosshard A, Regazzi R, Bernard C, Cuber JC, Takahashi M, et al. Expression of SNARE proteins in enteroendocrine cell lines and functional role of tetanus toxin-sensitive proteins in cholecystokinin release. FEBS Lett 1998;425:66–70.
[45] Bonifacino JS, Glick BS. The mechanisms of vesicle budding and fusion. Cell 2004;116:153–66.
[46] Okayama M, Arakawa T, Mizoguchi I, Tajima Y, Takuma T. SNAP-23 is not essential for constitutive exocytosis in HeLa cells. FEBS Lett 2007;581:4583–8.
[47] Tanigawara Y. Role of P-glycoprotein in drug disposition. Ther Drug Monit 2000;22:137–40.
[48] Kerr MC, Teasdale RD. Defining macropinocytosis. Traffic 2009;10:364–71.

OPEN ACCESS Freely available online

PLOS | ONE

Development of a Cell-Based Assay Measuring the Activation of FcγRIIa for the Characterization of Therapeutic Monoclonal Antibodies

Minoru Tada, Akiko Ishii-Watabe*, Takuo Suzuki, Nana Kawasaki

Division of Biological Chemistry and Biologicals, National Institute of Health Sciences, Tokyo, Japan

Abstract

Antibody-dependent cellular cytotoxicity (ADCC) is one of the important mechanisms of action of the targeting of tumor cells by therapeutic monoclonal antibodies (mAbs). Among the human Fcγ receptors (FcγRs), FcγRIIIa is well known as the only receptor expressed in natural killer (NK) cells, and it plays a pivotal role in ADCC by IgG1-subclass mAbs. In addition, the contributions of FcγRIIa to mAb-mediated cytotoxicity have been reported. FcγRIIa is expressed in myeloid effector cells including neutrophils and macrophages, and it is involved in the activation of these effector cells. However, the measurement of the cytotoxicity via FcγRIIa-expressing effector cells is complicated and inconvenient for the characterization of therapeutic mAbs. Here we report the development of a cell-based assay using a human FcγRIIa-expressing reporter cell line. The FcγRIIa reporter cell assay was able to estimate the activation of FcγRIIa by antigen-bound mAbs by a very simple method *in vitro*. The usefulness of this assay for evaluating the activity of mAbs with different abilities to activate FcγRIIa was confirmed by the examples including the comparison of the activity of the anti-CD20 mAb rituximab and its Fc-engineered variants, and two anti-EGFR mAbs with different IgG subclasses, cetuximab (IgG1) and panitumumab (IgG2). We also applied this assay to the characterization of a force-oxidized mAb, and we observed that oxidation significantly decreased the FcγRIIa activation by EGFR-bound cetuximab. These results suggest that our FcγRIIa reporter assay is a promising tool for the characterization of therapeutic mAbs, including Fc-engineered mAbs, IgG2-subclass mAbs, and their product-related variants.

Citation: Tada M, Ishii-Watabe A, Suzuki T, Kawasaki N (2014) Development of a Cell-Based Assay Measuring the Activation of FcγRIIa for the Characterization of Therapeutic Monoclonal Antibodies. PLoS ONE 9(4): e95787. doi:10.1371/journal.pone.0095787

Editor: Paul Zhou, Pasteur Institute of Shanghai, Chinese Academy of Science, China

Received January 9, 2014; **Accepted** March 28, 2014; **Published** April 21, 2014

Funding: This study was supported in part by the Advanced Research for Medical Products Mining Programme of the National Institute of Biomedical Innovation (NIBIO), by the Health and Labor Sciences Research Grants from the Ministry of Health, Labor, and Welfare of Japan, and by KAKENHI from the Japan Society for the Promotion of Science (JSPS). The funders had no role in study design, data collection and analysis, decision to publish, or preparation of the manuscript.

Competing Interests: The authors have declared that no competing interests exist.

* E-mail: watabe@nihs.go.jp

Introduction

Antibody-dependent cellular cytotoxicity (ADCC) plays an important role in anti-tumor activity of therapeutic monoclonal antibodies (mAbs) targeting tumor cells.[1–3] To date, many mAbs exhibiting ADCC activity have been approved and have contributed to anticancer therapy (e.g., the anti-EGFR (epidermal growth factor receptor) mAb cetuximab for colorectal cancers, the anti-CD20 mAb rituximab for B-cell lymphomas, and the anti-HER2 mAb trastuzumab for metastatic breast cancers). In addition, for the enhancement of ADCC activity, antibody Fc engineering by amino acid substitution [4–7] or glycoform modification [8–13] has been advanced. The glyco-engineered anti-CCR4 mAb mogamulizumab [14] and anti-CD20 mAb obinutuzumab [15] were recently approved in Japan and United States, respectively, and various Fc-engineered mAbs with higher ADCC activity are currently under development[16].

Activating Fcγ receptors (FcγRs) play a critical role in ADCC. mAbs bound to a cell-surface antigen interact with FcγRs expressed on effector cells such as natural killer (NK) cells, neutrophils and macrophages, inducing these cells to exert cytotoxicity. In humans, there are four types of activating FcγRs: FcγRI, FcγRIIa, FcγRIIIa and FcγRIIIb.[17] FcγRIIIa is the only activating FcγR expressed on NK cells, and it is thought to play a pivotal role in ADCC induced by IgG1 subclass mAbs. Its significance in clinical efficacy is supported by reports of correlations between FcγRIIIa polymorphism (F158V) and response to rituximab [18,19] or other mAbs. Much of the Fc engineering in tumor-targeting mAbs has increased the affinity to FcγRIIIa, resulting in enhanced ADCC activity via NK cells.

To assess ADCC activity of these mAbs, various methods of assaying ADCC have been reported. In most cases, the killing of target cells is measured by using human peripheral mononuclear blood cells (PBMCs) from donated blood or isolated primary NK cells as effector cells. Although these assays can directly assess the cytotoxicity induced by mAbs via effector cells, they have several drawbacks in their implementation for routine testing, such as the requirement of fresh blood from donors and insufficient repeatability caused by the differences in effector cell activity among donors. To resolve these problems, alternative assays to measure the binding or activation of FcγRIIIa by antigen-bound mAbs have been developed. Miller et al. reported that an enzyme-linked immunosorbent assay (ELISA)-based bridging assay using recombinant FcγRIIIa protein can be used as a surrogate assay for ADCC activity.[20] Parekh et al. developed an ADCC-reporter gene assay measuring the activation of FcγRIIIa-expressing

reporter cells with excellent performance in accuracy, precision and robustness.[21]

In addition to FcγRIIIa, the role of FcγRIIa in the efficacy of mAbs has been studied. Several clinical studies indicated the correlations between FcγRIIa polymorphism (R131H) and the response to IgG1 subclass mAbs such as rituximab [19] and cetuximab,[22] although the mechanism underlying these correlations is unclear because no significant difference was observed in the *in vitro* binding to human IgG1 between 131R and 131H alleles.[23] However, the importance of FcγRIIa in mAb-mediated cytotoxicity via immune effector cells other than NK cells has been reported. FcγRIIa is widely expressed in myeloid effector cells and plays a pivotal role in the activation of neutrophils [24–26] and macrophages.[6] Fc-engineered mAbs with higher FcγRIIa affinity by amino-acid substitutions have been developed, and their use succeeded in the enhancement of the mAb-mediated phagocytosis of tumor cells by macrophages [6].

In addition, FcγRIIa is a major receptor for IgG2 subclass mAbs. The IgG2-mediated elimination of infectious pathogens by myeloid effector cells plays an important role in protective immune responses. Thus, therapeutic IgG2-subclass mAbs may elicit effector functions via myeloid effector cells by FcγRIIa activation. Indeed, FcγRIIa was reported to be involved in the myeloid effector cell-mediated cytotoxicity by panitumumab, a human IgG2 mAb against EGFR.[27] Therefore, it is important to evaluate the mAb-dependent activation of FcγRIIa as well as that of FcγRIIIa in the development of tumor-targeting therapeutic mAbs of both the IgG1 and IgG2 subclasses. However, the main effector cells exerting ADCC in human PBMCs used for traditional ADCC assays are NK cells expressing FcγRIIIa, and these assays assess only the contribution of FcγRIIIa activation by mAbs. To assess the cytotoxicity via other effector cells expressing FcγRIIa, it is necessary to isolate primary neutrophils from fresh blood or to differentiate macrophages from primary monocytes and these processes may lead to variability of the assay.

The purpose of the present study was to establish a cell-based assay to conveniently measure mAb-dependent FcγRIIa activation. We developed an FcγRIIa-expressing reporter cell line in which the reporter luciferase gene expresses depending on the activation of FcγRIIa via crosslinking by antigen-bound mAbs. Cell-based assays using our reporter cell line are a promising tool for the assessment of Fc-engineered mAbs with different FcγRIIa-binding affinities or IgG2-subclass mAbs, and they would also be useful for the characterization of mAb product-related variants.

Materials and Methods

Cell Culture

Jurkat (RCB0806) cells were provided by the RIKEN BRC and cultured in RPMI1640 medium supplemented with 10% fetal bovine serum (FBS). Daudi (JCRB9071) and A431 (JCRB0004) cells were obtained from the JCRB cell bank. Daudi cells were cultured in RPMI1640 medium supplemented with 20% FBS. A431 cells were cultured in DMEM high glucose with GlutaMAX (Life Technologies) supplemented with 10% FBS and 1 mM sodium pyruvate.

Establishment of the Jurkat/FcγR/NFAT-Luc Cell Line

We generated cDNA encoding human FcγRIIa/131H by an inverse polymerase chain reaction (PCR) method using cDNA encoding FcγRIIa/131R (Open Biosystems) as a template and subcloned into pVITRO1-neo-mcs vector (InvivoGen). We subcloned cDNA encoding human FcγRIIIa/158V (OriGene) and Fcγ chain (Open Biosystems) into pVITRO1-neo-mcs vector. Jurkat cells were transfected with pVITRO1-neo-FcγRIIa/131H or pVITRO1-neo-FcγRIIIa/158V+Fcγ chain by Nucleofector (Lonza).

Stable cell lines expressing FcγRIIa or both FcγRIIIa and Fcγ chain were screened by selection using 500 μg/mL G418 (Nacalai Tesque) and the limited dilution method, followed by a flow cytometric analysis to confirm the expression of FcγRs. To generate the cell line co-expressing NFAT-driven luciferase reporter gene, we transfected Jurkat/FcγRIIa and Jurkat/FcγRIIIa cells with pGL4.30[*luc2P*/NFAT-RE/Hygro] vector (Promega) containing hygromycin-resistance gene. We confirmed the activation of NFAT-driven luciferase reporter by conducting FcγR-crosslinking assays using anti-FcγR antibodies.

Flow Cytometric Analysis

We analyzed the cell surface expression of FcγRs using the FACSCanto II flow cytometer (BD Biosciences, San Diego, CA) using fluoresceine-isothiocyanate (FITC)-conjugated anti-CD32 monoclonal antibody (clone FLI8.26, BD Biosciences) or anti-CD16 monoclonal antibody (clone 3G8, BD Biosciences). For the flow cytometry-based bridging assay, Daudi and Jurkat/FcγRs cells were labeled with Calcein AM (eBioscience) and Calcein Violet 450 AM (eBioscience) respectively according to the manufacturer's instructions. Fluorescently-labeled Daudi (3×10^4 cells/well) and Jurkat/FcγRs (3×10^5 cells/well) were co-cultured in a 96-well plate for 30 min in the presence of 10 μg/mL rituximab or control human IgG1 (SIGMA), and then analyzed by the FACSCanto II flow cytometer.

FcγR Crosslinking Assay

We performed the FcγR crosslinking assay as described.[28] Jurkat/FcγRs cells were washed with Opti-MEM I Reduced Serum Media (Life Technologies) and incubated on ice for 30 min with the medium containing 15 μg/mL mouse anti-FcγRs monoclonal antibody: anti-CD32 (clone IV.3, StemCell Technologies,) or anti-CD16 (clone 3G8, BD Biosciences). After being washed three times with the medium, the cells were suspended in the medium and warmed to 37°C for 10 min, and then crosslinked by goat F(ab') 2 anti-mouse IgG (Beckman Coulter), followed by incubation at 37°C. At each time point, the cells were lysed by adding (2×) lysis buffer (100 mM Tris-HCl, pH 7.5, 300 mM NaCl, 2% Nonidet-P40, 0.5% deoxycholate, (2×) Protease Inhibitor Cocktail [Nacalai Tesque], and (2×) Phosphatase Inhibitor Cocktail [Nacalai Tesque]) and centrifuged at 20,000 g for 15 min at 4°C. The supernatants were subjected to sodium dodecyl sulfate polyacrylamide gel electrophoresis (SDS-PAGE), followed by immunoblotting with horseradish peroxidase (HRP)-conjugated anti-phosphorylated tyrosine antibody (clone pY20, GE Healthcare,). Chemiluminescence was detected using Super Signal West Femto Chemiluminescent Substrate (Pierce) and the ImageQuant LAS 4000 mini digital imaging system (GE Healthcare).

For the measurement of the activation of Jurkat/FcγR/NFAT-Luc cells, Jurkat/FcγR/NFAT-Luc cells were crosslinked by anti-CD32 or anti-CD16 antibody as described above, and incubated at 37°C in 5% CO_2. At each time point, the luciferase activities were measured by using ONE-Glo Luciferase Assay System (Promega) and the EnSpire Multimode Plate Reader (PerkinElmer).

Antibodies

DNA fragments encoding the rituximab heavy-chain and light-chain variable domains were synthesized by Integrated DNA

Technologies, and subcloned into pFUSE-CHIg-hG1 and pFUSE2-CLIg-hk vector (InvivoGen), respectively. The expression vectors encoding the rituximab Fc variants with G236A/S239D/I332E or L234A/L235A substitutions were constructed by using synthesized DNA fragments. Rituximab and its Fc variants were expressed using the FreeStyle MAX CHO Expression System (Life Technologies).Briefly, CHO-S cells were co-transfected with the plasmid vectors expressing rituximab heavy chain and light chain by using the FreeStyle MAX Reagent, and they were then cultured for 6 days in FreeStyle CHO Expression Medium. The cell culture supernatant was collected by centrifugation (400 g for 10 min) and applied to a HiTrap Protein G HP column (GE Healthcare) equilibrated with 20 mM phosphate buffer (pH 6.8). After the column was washed with 20 mM phosphate buffer (pH 6.8), mAbs were eluted by 0.1 M Glycine-HCl (pH 3.0) and neutralized by 1 M Tris-HCl (pH 8.0), followed by desalting using a PD-10 column (GE Healthcare) equilibrated with phosphate-buffered saline (PBS). The concentration of purified mAb was determined by spectrophotometry using the NanoDrop 2000c spectrophotometer (Thermo Scientific). Cetuximab (Erbitux, Merck Serono) and panitumumab (Vectibix, Amgen) were purchased via reagent distributors.

ADCC Assay

Cryopreserved human PBMCs were obtained from Cellular Technology Limited, and thawed just before ADCC assay according to the manufacturer's protocol. Daudi (1×10^4 cells/well) and human PBMC (2×10^5 cells/well) suspended in CTL-Test Medium (Cellular Technology Limited) were seeded in a 96-well plate with serially diluted rituximab. After incubation for 4 hr at 37°C in 5% CO_2, lactate dehydrogenase (LDH) activity of cell culture supernatants were measured by using Cytotoxicity Detection Kit^{PLUS} (LDH) (Roche Applied Science). The percentage cytotoxicity was calculated as described in the manufacturer's protocol. The ethical review boards of the National Institute of Health Sciences approved the use of human PBMC in this study.

FcγR Reporter Assay

Daudi (2×10^4 cells/well) and Jurkat/FcγRs/NFAT-Luc (1×10^5 cells/well) suspended in Opti-MEM I Reduced Serum Media were seeded in a 96-well plate with serially diluted rituximab. After incubation for 5 hr at 37°C in 5% CO_2, we measured the luciferase activities by using ONE-Glo Luciferase Assay System (Promega) and the EnSpire Multimode Plate Reader (PerkinElmer).

For the assays using anti-EGFR mAbs, A431 (2×10^4 cells/well) were seeded in a 96-well plate and cultured for 24 hr at 37°C in 5% CO_2. After the medium was removed, Jurkat/FcγRs/NFAT-Luc (1×10^5 cells/well) suspended in Opti-MEM I Reduced Serum Media were added with serially diluted anti-EGFR mAbs and incubated for 5 hr, followed by measurement of the luciferase activity as described above.

Forced Oxidization of Cetuximab by t-BHP

Cetuximab (5 mg/mL) was incubated in PBS containing 0.2, 1 or 5% of tert-Butyl hydroperoxide (t-BHP) (Wako) for 3 hr at 37°C. After the incubation, t-BHP was removed from the reaction mixtures by applying the mixtures two times to a PD Spin Trap G-25 column (GE Healthcare) equilibrated with PBS.

SPR Analysis

A Biacore T200 SPR biosensor (GE Healthcare) and CM5 sensor chip were used to evaluate the binding properties of mAbs. All measurements were performed at 25°C, with a flow rate of 30 μL/min for analytes. The binding affinity of mAbs with FcRn was measured as described.[29] Briefly, the recombinant human FcRn was immobilized onto a sensor chip (GE Healthcare) by the amine coupling method (~350 RU). The mAb samples in twofold serial dilutions from 670 to 42 nM with the running buffer (50 mM sodium phosphate/150 mM NaCl [pH 6.0]) were injected for 120 sec followed by a 150-sec dissociation phase.

The surface was regenerated by injecting the buffer of 100 mM Tris with 200 mM NaCl [pH 8.0] for 30 sec. The dissociation constant (K_D) was calculated from the sensorgrams using the bivalent analyte model and setting the bulk reflective index to zero using BICORE T200 evaluation software (GE Healthcare). We measured the affinities of mAbs with human FcγRIIa and FcγRIIIa using the sensor chip with which the recombinant ectodomains of human FcγRIIa or FcγRIIIa (Sino Biological) were immobilized by the amine coupling method.

mAb samples in twofold serial dilutions with HBS-EP buffer (50 mM sodium phosphate/150 mM NaCl [pH 6.0]) were injected for 3 min followed by a 4-min dissociation phase. The analyte concentrations were from 2680 to 21 nM and from 335 to 21 nM for FcγRIIa and FcγRIIIa, respectively. The surface was regenerated by injecting 10 mM NaOH for 30 sec. The dissociation constant K_D for FcγRIIa was calculated by the steady-state method. The dissociation constant K_D for FcγRIIIa was calculated by the two-state model[30].

For the measurement of the binding affinity with EGFR, anti-human IgG antibody (GE Healthcare) was immobilized onto sample and reference flow cells of a sensor chip. A mAb sample (0.2 μg/mL) was captured on a sensorchip by injecting it into the sample flow cell at a flow rate of 10 μL/min for 1 min. The recombinant ectodomain of human EGF receptor (Sino Biological) in twofold serial dilutions from 40 to 2.5 nM with HBS-EP buffer was injected for 5 min followed by a 10-min dissociation phase. After each cycle, the surface was regenerated by injecting 3 M $MgCl_2$ for 30 sec. The dissociation constant K_D for EGFR was calculated using the 1:1 binding model. In all experiments, each binding sensorgram from the sample flow cell was corrected for both the surface blank and the buffer injection control (double reference).[31] Statistical analysis was performed using one-way analysis of variance (ANOVA) with Tukey's multiple comparison test (PRISM version 5.02; Graphpad Software).

Results

Establishment of FcγR-expressing Reporter Cell Lines

To develop the reporter cell lines measuring FcγRs activation, we first generated the Jurkat cell line which stably expresses FcγRIIa (Jurkat/FcγRIIa). The cell line expressing FcγRIIIa (Jurkat/FcγRIIIa) was also established. The specific expression of FcγR in each cell line was confirmed by a flow cytometric analysis (Fig. 1A). We next examined whether these cell lines were activated via the crosslinking of FcγRs. The crosslinking of FcγRs by immune complexes induces the phosphorylation of immunoreceptor tyrosine-based activation motif (ITAM) located on the cytoplasmic tail of the FcγRs, which triggers the activation of a downstream signaling pathway[17].

As shown in Figure 1B, the crosslinking of FcγRs by anti-FcγRs antibodies increased the tyrosine-phosphorylated proteins in the Jurkat/FcγR cells, indicating that both Jurkat/FcγRIIa and Jurkat/FcγRIIIa cells are responsive to FcγR stimulation. To exert ADCC, FcγRs-expressing effector cells recognize the mAbs bound to antigen on the surface of target cells. This bridging of target and effector cells by the mAbs is a critical step for the

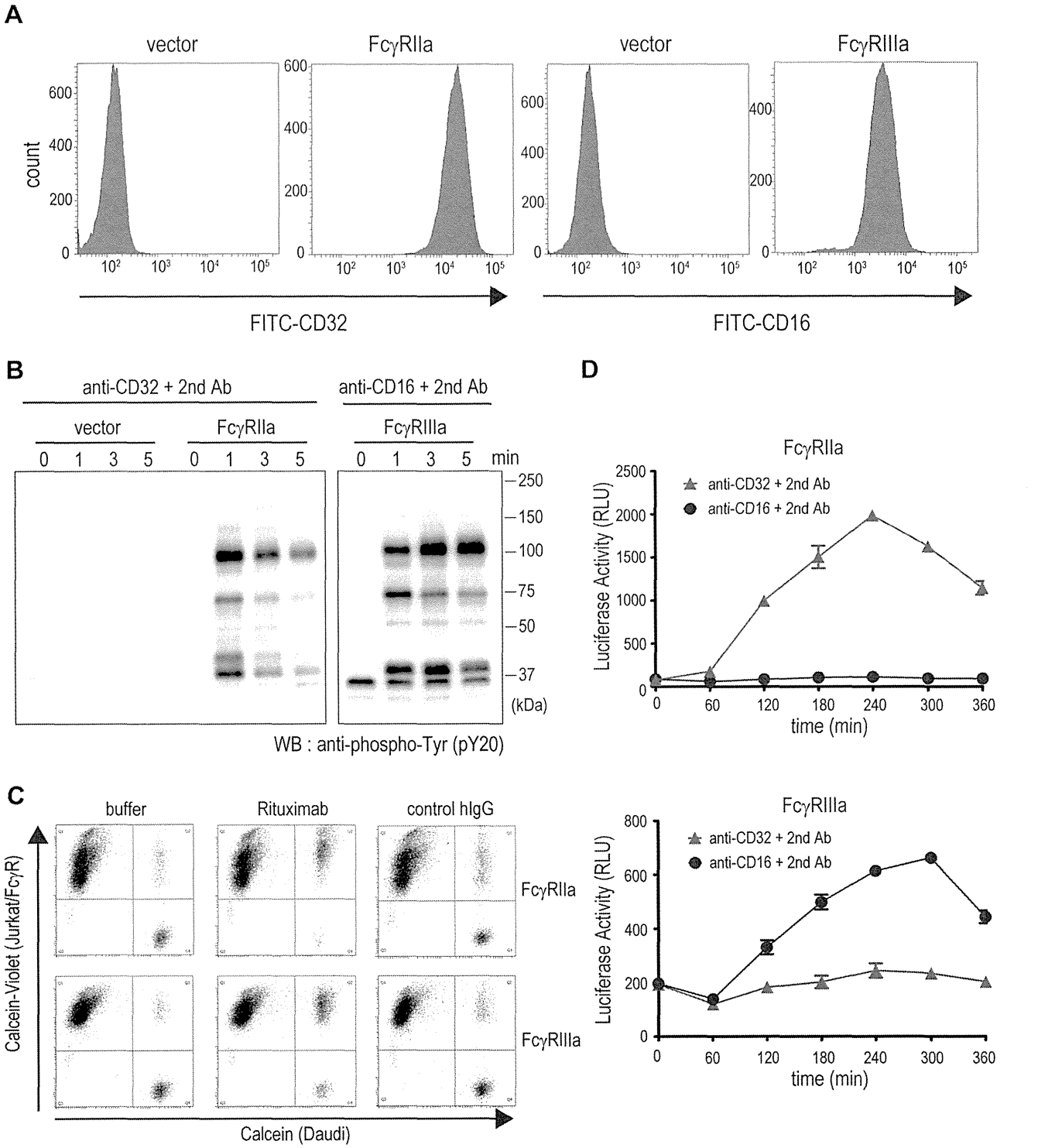

Figure 1. Establishment of the FcγR-expressing reporter cell lines. (A) The cell surface expressions of FcγRs in Jurkat/FcγR cells were analyzed by flow cytometric analysis. (B) The crosslinking of FcγRs by anti-FcγR monoclonal antibodies induced the tyrosine-phosphorylated proteins in Jurkat/FcγR cells. (C) Bridging between calcein-labeled Daudi and calcein-violet-labeled Jurkat/FcγR cells via rituximab was analyzed by flow cytometry. (D) The crosslinking of FcγRs by anti-FcγR monoclonal antibodies induced the luciferase activities in Jurkat/FcγR/NFAT-Luc cells. The assays were performed in triplicate, and the data are the mean ± SEM.
doi:10.1371/journal.pone.0095787.g001

initiation of ADCC. To assess the bridging ability of Jurkat/FcγR cells, we performed the flow cytometry-based bridging assay. Calcein-labeled Daudi cells, a human Burkitt's lymphoma cell line that strongly expresses CD20, and calcein-violet-labeled Jurkat/FcγR cells were co-incubated with or without an anti-CD20 mAb (rituximab) and analyzed by flow cytometry.

With the addition of rituximab, the calcein/calcein-violet double-positive population was significantly increased (Fig. 1C), indicating that the Jurkat/FcγR cells recognized rituximab bound to CD20 at the surface of the Daudi cells; that is, Daudi and Jurkat/FcγR cells were bridged by rituximab. These results suggest that the Jurkat/FcγRIIa and Jurkat/FcγRIIIa cell lines we developed can function as reporter cells mimicking FcγR-expressing immune cells such as NK cells and macrophages.

To monitor the activation of Jurkat/FcγR cells conveniently, we introduced the luciferase reporter gene driven by NFAT-response element (NFAT-RE) into Jurkat/FcγR cells and established the reporter cell lines Jurkat/FcγRIIa/NFAT-Luc and Jurkat/FcγRIIIa/NFAT-Luc. NFAT is a well-known transcription factor activated by intracellular calcium signaling, and the reporter gene driven by NFAT-RE has been known as a useful tool for monitoring FcγR activation.[21] We confirmed that the luciferase reporter was activated via the crosslinking of FcγRs by anti-FcγRs antibodies (Fig. 1D).

Measurement of mAb-dependent FcγRIIa Activation by Using Jurkat/FcγRIIa/NFAT-Luc

To assess the usefulness of Jurkat/FcγRIIa/NFAT-Luc cells for the measurement of mAb-dependent FcγRIIa activation, we first performed the assay using anti-CD20 mAb rituximab and its engineered Fc variants with increased or decreased affinities to FcγRs. The engineered Fc variant with G236A/S239D/I332E substitutions has been reported to exhibit higher FcγRIIa and FcγRIIIa binding and enhanced activation of effector cells, including NK cells and macrophages.[6] On the other hand, the variant with L234A/L235A substitutions is known to bind FcγRs weakly and activate effector cells with lower efficiency.[32] We confirmed that the rituximab G236A/S239D/I332E variant exhibit ADCC activity more strongly than wild-type rituximab, whereas the rituximab L234A/L235A variant exhibit lower ADCC activity than wild-type rituximab (Fig. 2A).

We found that the luciferase activity of Jurkat/FcγRIIa/NFAT-Luc cells as well as Jurkat/FcγRIIIa/NFAT-Luc cells was dose-dependently increased by rituximab in co-culture with Daudi cells (Fig. 2B), suggesting that the activation of FcγRIIa by the bridging of target and effector cells via mAbs can be assessed by using Jurkat/FcγRIIa/NFAT-Luc cells. Furthermore, the Jurkat/FcγRIIa/NFAT-Luc cells were activated by the rituximab G236A/S239D/I332E variant more strongly than wild-type rituximab, whereas they were hardly activated by the rituximab L234A/L235A variant. Similar results were observed by using Jurkat/FcγRIIIa/NFAT-Luc cells (Fig. 2B).

We next performed the assay using A431 cells (a human epithelial carcinoma cell line that overexpresses EGFR) as target cells and two anti-EGFR mAbs, cetuximab and panitumumab. Cetuximab is a human-mouse chimeric IgG1 mAb, and panitumumab is a fully human IgG2 mAb. Regarding the characteristics of the human IgG subclass, IgG1 binds FcγRIIIa and exhibits ADCC efficiently by NK cells, whereas IgG2 shows weak binding activity to FcγRIIIa.

Panitumumab has been thought to be inactive regarding the induction of ADCC. However, Schneider-Merck and coworkers reported that panitumumab exerted ADCC by myeloid effector cells (i.e., neutrophils and monocytes) isolated from human blood, and that the cytotoxicity may be triggered by FcγRIIa.[27] As shown in Figure 3, cetuximab (IgG1) activated the Jurkat/FcγRIIIa/NFAT-Luc cells effectively in a dose-dependent manner, whereas panitumumab (IgG2) did not. Both cetuximab and panitumumab activated Jurkat/FcγRIIa/NFAT-Luc cells, and the activity of panitumumab was significantly higher than that of

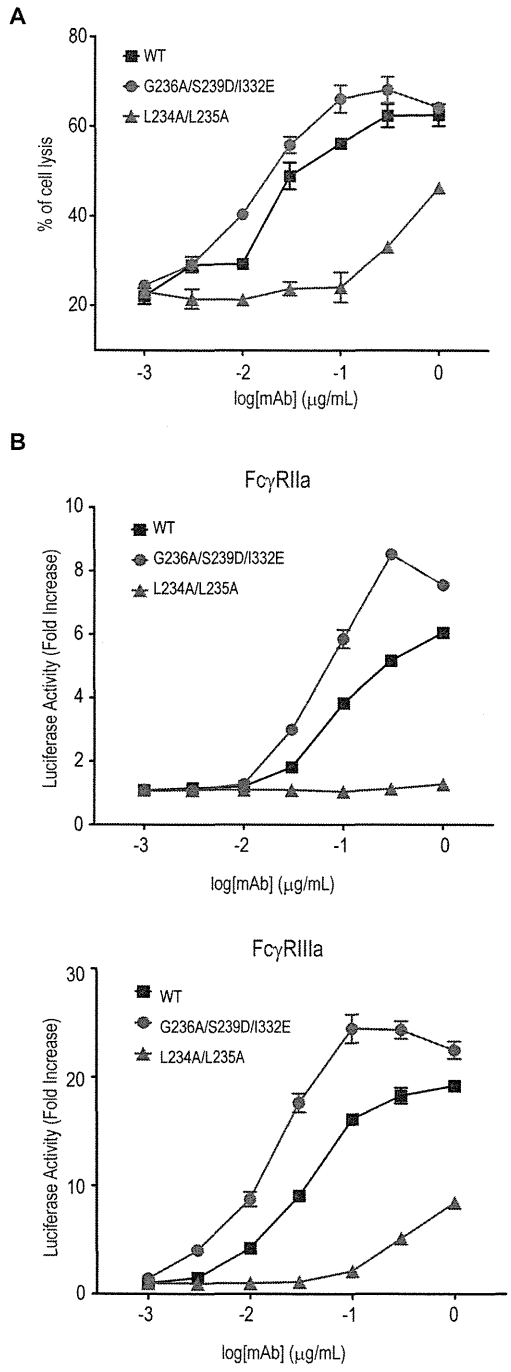

Figure 2. Activation of Jurkat/FcγR/NFAT-Luc cells by CD20-bound rituximab. (A) Daudi and human PBMC were co-cultured (the effector to target cell ratio was 20:l) in the presence of serially diluted rituximab or its Fc-engineered variants: G236A/S239D/I332E with higher FcγR binding and L234A/L235A with lower FcγR binding. Percentage cytotoxicity calculated by LDH activity released from damaged cells is represented on the graphs. The assays were performed in triplicate, and the data are the mean ± SEM. The rituximab G236A/S239D/I332E variant exhibited ADCC activity (EC_{50} = 0.013 μg/ml) more strongly than wild-type rituximab (EC_{50} = 0.023 μg/ml) ($p<0.05$, Graphpad Prism Software). (B) Daudi and Jurkat/FcγR/NFAT-Luc cells were co-cultured in the presence of serially diluted rituximab or its Fc-engineered variants. Luciferase activity (i.e., the fold increase compared to the control sample without mAbs) is represented on the graphs. The assays were performed in triplicate, and the data are the mean ± SEM. Jurkat/FcγRIIa/NFAT-Luc cells were activated by the rituximab G236A/S239D/

I332E variant (EC_{50} = 0.057 μg/ml) more strongly than wild-type rituximab (EC_{50} = 0.094 μg/ml) ($p<0.005$, Graphpad Prism Software). Jurkat/FcγRIIIa/NFAT-Luc cells were activated by the rituximab G236A/S239D/I332E variant (EC_{50} = 0.016 μg/ml) more strongly than wild-type rituximab (EC_{50} = 0.034 μg/ml) ($p<0.0001$, Graphpad Prism Software).
doi:10.1371/journal.pone.0095787.g002

cetuximab. These results were consistent with those of the previous study [27] using primary cultured effector cells, suggesting that the Jurkat/FcγRIIa/NFAT-Luc cell lines are useful for estimating the potency of IgG2 mAbs to activate FcγRIIa-expressing effector cells.

Impact of Oxidation on the Ability of Cetuximab to Activate FcγRs

To estimate the usefulness of Jurkat/FcγRIIa/NFAT-Luc and Jurkat/FcγRIIIa/NFAT-Luc cells in mAbs-variant characterization, we analyzed the impact of methionine oxidation on the ability of cetuximab to activate FcγRs. Methionine oxidation in IgG Fc is known to decrease the affinity of IgG for FcRn, an Fc receptor regulating IgG recycling in endothelial and blood cells, which leads to reduce the serum half-life of IgG.[33–35] However, the effects of methionine oxidation in IgG Fc on FcγR activation are not fully understood.

To prepare the samples with different levels of oxidation, cetuximab was treated with tert-butyl hydroperoxide (t-BHP), which is known to oxidate methionine residues preferentially in proteins, at different concentrations. Surface plasmon resonance (SPR) analysis using these oxidized mAbs showed that the binding affinity of cetuximab for FcRn was decreased in a dose-dependent manner by t-BHP (Fig. 4A), suggesting that t-BHP treatment dose-dependently induced methionine oxidation in Fc region of cetuximab.

On the other hand, t-BHP treatment induced only a slight decrease in the binding activities of cetuximab for EGFR, FcγRIIa and FcγRIIIa (Fig. 4A). We next performed the cell-based reporter assay using Jurkat/FcγRIIa/NFAT-Luc and Jurkat/FcγRIIIa/NFAT-Luc cells to estimate the effect of oxidation in cetuximab Fc on antigen-binding-dependent FcγR activation. In contrast to the *in vitro* binding analysis using SPR, we found that the t-BHP treatment significantly diminished the FcγRIIa activation by EGFR-bound cetuximab, although FcγRIIIa activation was not influenced by t-BHP treatment (Fig. 4B). These results suggest that methionine oxidation may decrease the FcγRIIa activation by EGFR-bound cetuximab and that Jurkat/FcγRIIa/NFAT-Luc cells are useful for monitoring the changes of mAb biological activities.

Discussion

Cell-based assays reflecting mechanisms of action are indispensable for assessing the biological activities of therapeutic mAbs from the early stage of drug discovery to post-approval quality control tests. In association with the progress in the development of tumor-targeting mAbs and their engineered variants with higher ADCC activity, various methods of measuring ADCC have been developed.[20,21,36–38] However, most of these assay methods were designed to estimate ADCC mediated by NK cells via FcγRIIIa, and the contribution of FcγRIIa was hardly detected.

Considering the importance of FcγRIIa-mediated cytotoxicity by mAbs, in the present study we developed a cell-based assay using Jurkat/FcγRIIa/NFAT-Luc reporter cells. The FcγRIIa-reporter assay can measure the activation of FcγRIIa by antigen-bound mAbs, and is a promising tool for estimating the tumor-targeting mAbs and their Fc-engineered variants with enhanced or decreased FcγRIIa-binding affinity.

During the development of therapeutic mAbs, IgG subclass selection and the evaluation of their interactions with FcγRs are important issues. Among the human IgG subclasses, IgG1 is the most commonly used subclass for therapeutic mAbs. In particular, the effector functions of IgG1 (i.e., the induction of ADCC and complement-dependent cytotoxicity) are important for the mAbs inducing tumor-cell killing, and Fc engineering technologies enhancing the effector functions of IgG1 have been applied to the development of novel anti-cancer therapeutic mAbs.

However, immune reactions mediated by complement or FcγR activation can sometimes be responsible for the adverse reactions by unwanted cytotoxicity to antigen-expressing cells or unwanted activation of effector cells. Therefore, when target-cell killing via effector function is not required, IgG4 is a preferable subclass to reduce the unwanted immune reactions, because IgG4 induces effector functions more weakly than IgG1. IgG2 has also been thought to be the isotype of choice for mAbs not requiring immune reactions because of its inability to activate the classical complement pathway and bind to activating FcγRs (FcγRI and

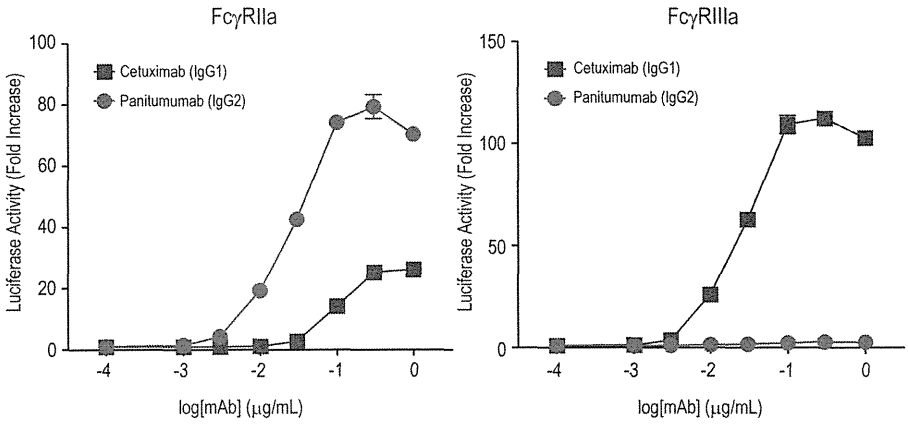

Figure 3. Activation of Jurkat/FcγR/NFAT-Luc cells by EGFR-bound cetuximab and panitumumab. A431 and Jurkat/FcγR/NFAT-Luc cells were co-cultured in the presence of serially diluted cetuximab (IgG1 subclass) or panitumumab (IgG2 subclass). The luciferase activity (i.e., the fold increase compared to the control sample without mAbs) is represented on the graphs. The assays were performed in triplicate, and the data are the mean ± SEM. Panitumumab activated Jurkat/FcγRIIa/NFAT-Luc cells more strongly than cetuximab ($p<0.0001$, Graphpad Prism Software).
doi:10.1371/journal.pone.0095787.g003

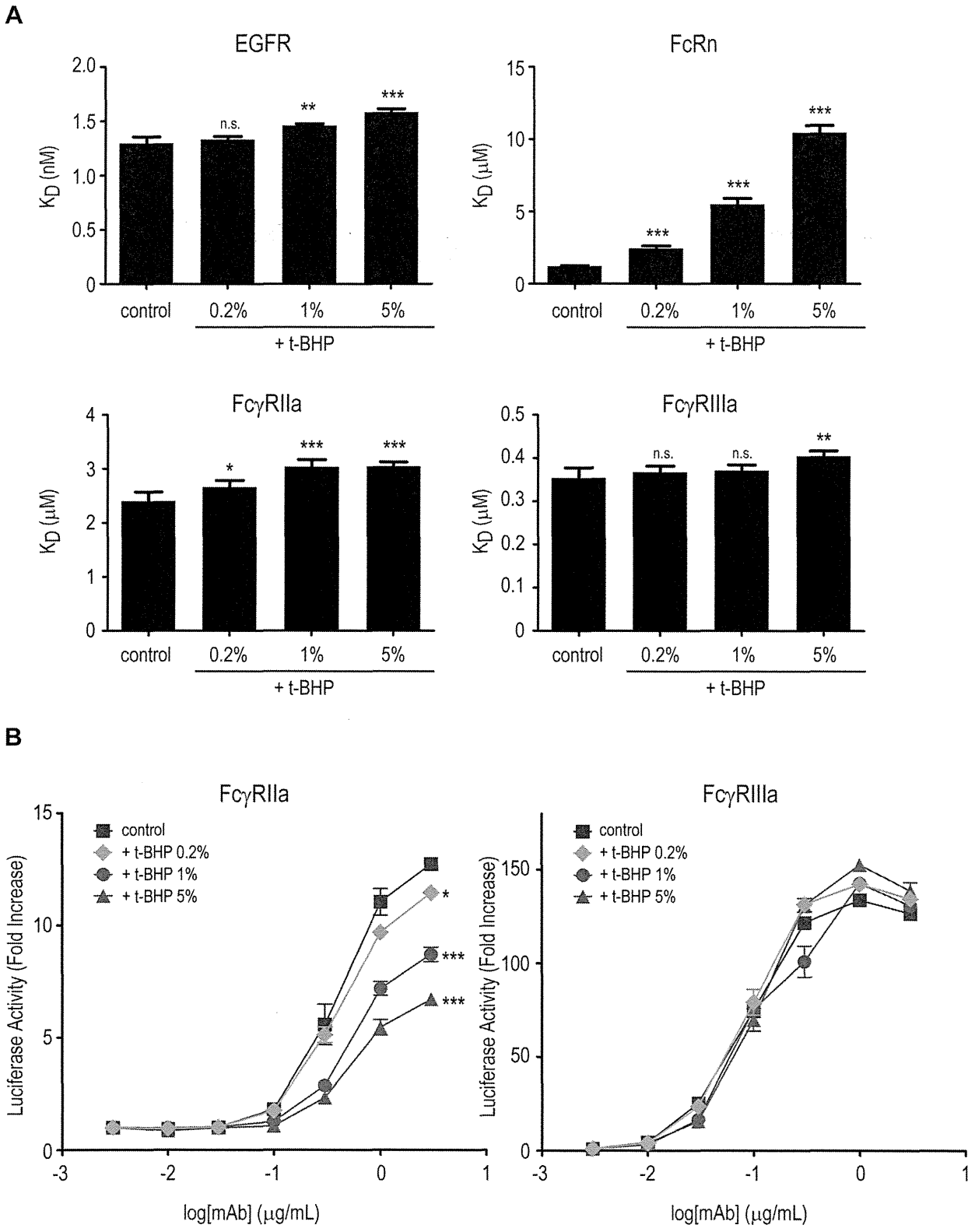

Figure 4. Effects of methionine oxidation on the activation of FcγRIIa and FcγRIIIa by cetuximab. (A) Binding affinities of t-BHP-treated cetuximab to EGFR, FcRn, FcγRIIa and FcγRIIIa were measured by an SPR analysis. Dissociation constant (K_D) values are represented as mean ± SD (n = 3). *, $p<0.05$; **, $p<0.01$; ***, $p<0.005$; n.s, not significant. (B) Activation of FcγRIIa and FcγRIIIa by t-BHP-treated cetuximab was measured by an FcγR reporter assay using A431 cells as target cells. Methionine oxidation caused by t-BHP treatment dose-dependently decreased the activation of FcγRIIa (*, $p<0.05$; ***, $p<0.005$), but not that of FcγRIIIa (not significant).
doi:10.1371/journal.pone.0095787.g004

FcγRIIIa).[23,39] However, IgG2 binds FcγRIIa, which is widely expressed in myeloid effector cells including monocytes, macrophages and neutrophils, and IgG2 immune complexes activate these effector cells via FcγRIIa crosslinking.

The activation of FcγRIIa is thought to be involved not only in the efficacy but also in the safety of therapeutic mAbs. Therapeutic mAbs sometimes induce infusion and hypersensitivity reactions, which are generic terms for acute adverse reactions that can be caused by an immunologic mechanism, including cytokine-release syndrome (CRS), allergic reactions, and pseudoallergic reactions.[40,41] There are some putative molecular mechanisms in which mAbs cause the release of inflammatory cytokines. mAbs targeting the cell-surface antigens expressed in immune cells may induce the cytokine release from the target cells by agonistic activity (e.g., muromonab-CD3 [42] and TGN1412 [43]). Therapeutic mAbs also have the potential to trigger cytokine release by an interaction with activating FcγRs on immune effector cells, regardless of whether or not target cell killing is required for their pharmacological activities. The involvement of FcγRIIa in cytokine release and the adverse effects of murine anti-CD3 antibody were reported by Tax et al.[44] In addition, the contribution of FcγRIIa to IgG-induced allergic reactions and anaphylaxis was recently reported by Jönsson et al.[45,46] Those researchers found that FcγRIIa was sufficient to trigger active and passive anaphylaxis in an FcγRIIa-transgenic mice model, and human mast cells, monocytes and neutrophils produced an anaphylactogenic mediator by FcγRIIa crosslinking.

These findings suggest the importance of activating FcγRs in the pathogenic mechanisms of infusion and hypersensitivity reactions by therapeutic mAbs. Thus, when considering the safety profiles of therapeutic mAbs, it is necessary to evaluate the activation of FcγRs by the mAbs. As described above, FcγRIIa is expressed widely in myeloid effector cells including neutrophils, and it is thought to play a pivotal role in the activation of these cells. Our FcγRIIa-reporter assay can measure the activation of FcγRIIa by antigen-bound mAbs *in vitro*, and may contribute to the assessment of the safety profile of therapeutic mAbs.

In the present study, we also showed the usefulness of the FcγR-reporter assay for the characterization of mAb variants. Oxidation is one of the most common modifications that occur during the manufacturing and storage processes of therapeutic proteins.[47,48] Among the various amino acid residues which can be oxidized, methionine is the most sensitive residue to oxidation. Human IgG1 contains two conserved methionine residues (Met-252 and Met-428) in its constant region. Previous studies revealed that methionine oxidation induces structural changes in the IgG Fc region,[49] decreases the binding affinity to FcRn,[33,34] and reduces the serum half-life of IgG[43].

However, the effects of methionine oxidation on the ability of mAbs to activate FcγRs have not been fully understood, although a subtle decrease in FcγRIIa binding was observed in methionine-oxidized trastuzumab.[33] We reported here that oxidation in cetuximab significantly decreased the EGFR binding-dependent activation of FcγRIIa-expressing reporter cells, but not that of FcγRIIIa-expressing reporter cells. Interestingly, oxidation induced only a slight change in the binding affinities to EGFR and FcγRIIa in an SPR analysis using recombinant proteins.

There are two potential mechanisms to explain the difference between the results of the *in vitro* binding assay and those of the cell-based assay: first, that the slight decrease in the binding affinity to both EGFR and FcγRIIa observed in the SPR analysis may have synergistically affected the FcγRIIa-activation in the cell-based assay; and second, that oxidation may influence the structural changes at the Fc region caused by antigen binding, resulting in the reduced efficacy of EGFR-bound cetuximab to activate FcγRIIa. In both cases, the cell-based assay mimicking the *in vivo* situation is thought to be superior to the *in vitro* binding assay using recombinant proteins when characterizing the biological activities of mAb variants. To our knowledge, this is the first report demonstrating the effect of methionine oxidation on the efficacy of mAbs to activate FcγRs. Further studies are required to reveal the detailed mechanisms underlying the effects of methionine oxidation on the structure of mAbs' Fc region and its functions.

In conclusion, we reported here the development of a cell-based assay using an FcγRIIa-expressing reporter cell line. Our FcγRIIa reporter cell assay can evaluate the activation of FcγRIIa by antigen-bound mAbs *in vitro* and is useful for the characterization of therapeutic mAbs, including Fc-engineered mAbs, IgG2-subclass mAbs, and their product-related variants. Although further studies are required to reveal a correlation between *in vivo* efficacy and *in vitro* FcγRIIa activation, as is true of the previously reported FcγRIIIa reporter cell assay, our FcγRIIa reporter cell assay is a promising tool for the characterization of therapeutic mAbs.

Acknowledgments

We thank Ms. Chizuru Miyama for technical assistance.

Author Contributions

Conceived and designed the experiments: MT AI TS. Performed the experiments: MT AI TS. Analyzed the data: MT AI TS. Contributed reagents/materials/analysis tools: MT AI TS. Wrote the paper: MT AI TS NK.

References

1. Alderson KL, Sondel PM (2011) Clinical cancer therapy by NK cells via antibody-dependent cell-mediated cytotoxicity. J Biomed Biotechnol 2011: 379123.
2. Scott AM, Allison JP, Wolchok JD (2012) Monoclonal antibodies in cancer therapy. Cancer Immun 12: 14.
3. Weiner LM, Surana R, Wang S (2010) Monoclonal antibodies: versatile platforms for cancer immunotherapy. Nat Rev Immunol 10: 317–327.
4. Lazar GA, Dang W, Karki S, Vafa O, Peng JS, et al. (2006) Engineered antibody Fc variants with enhanced effector function. Proc Natl Acad Sci U S A 103: 4005–4010.
5. Mimoto F, Igawa T, Kuramochi T, Katada H, Kadono S, et al. (2013) Novel asymmetrically engineered antibody Fc variant with superior FcgammaR binding affinity and specificity compared with afucosylated Fc variant. MAbs 5: 229–236.
6. Richards JO, Karki S, Lazar GA, Chen H, Dang W, et al. (2008) Optimization of antibody binding to FcgammaRIIa enhances macrophage phagocytosis of tumor cells. Mol Cancer Ther 7: 2517–2527.
7. Strohl WR (2009) Optimization of Fc-mediated effector functions of monoclonal antibodies. Curr Opin Biotechnol 20: 685–691.
8. Ferrara C, Brunker P, Suter T, Moser S, Puntener U, et al. (2006) Modulation of therapeutic antibody effector functions by glycosylation engineering: influence of Golgi enzyme localization domain and co-expression of heterologous beta1, 4-N-acetylglucosaminyltransferase III and Golgi alpha-mannosidase II. Biotechnol Bioeng 93: 851–861.
9. Davies J, Jiang L, Pan LZ, LaBarre MJ, Anderson D, et al. (2001) Expression of GnTIII in a recombinant anti-CD20 CHO production cell line: Expression of antibodies with altered glycoforms leads to an increase in ADCC through higher affinity for FC gamma RIII. Biotechnol Bioeng 74: 288–294.
10. Satoh M, Iida S, Shitara K (2006) Non-fucosylated therapeutic antibodies as next-generation therapeutic antibodies. Expert Opin Biol Ther 6: 1161–1173.
11. Shields RL, Lai J, Keck R, O'Connell LY, Hong K, et al. (2002) Lack of fucose on human IgG1 N-linked oligosaccharide improves binding to human Fcgamma RIII and antibody-dependent cellular toxicity. J Biol Chem 277: 26733–26740.
12. Shinkawa T, Nakamura K, Yamane N, Shoji-Hosaka E, Kanda Y, et al. (2003) The absence of fucose but not the presence of galactose or bisecting N-

acetylglucosamine of human IgG1 complex-type oligosaccharides shows the critical role of enhancing antibody-dependent cellular cytotoxicity. J Biol Chem 278: 3466–3473.
13. Zhou Q, Shankara S, Roy A, Qiu H, Estes S, et al. (2008) Development of a simple and rapid method for producing non-fucosylated oligomannose containing antibodies with increased effector function. Biotechnol Bioeng 99: 652–665.
14. Subramaniam JM, Whiteside G, McKeage K, Croxtall JC (2012) Mogamulizumab: first global approval. Drugs 72: 1293–1298.
15. Traynor K (2013) Obinutuzumab approved for CLL: Monoclonal antibody product is first FDA-approved breakthrough therapy. Am J Health Syst Pharm 70: 2162.
16. Desjarlais JR, Lazar GA, Zhukovsky EA, Chu SY (2007) Optimizing engagement of the immune system by anti-tumor antibodies: an engineer's perspective. Drug Discov Today 12: 898–910.
17. Nimmerjahn F, Ravetch JV (2008) Fcgamma receptors as regulators of immune responses. Nat Rev Immunol 8: 34–47.
18. Cartron G, Dacheux L, Salles G, Solal-Celigny P, Bardos P, et al. (2002) Therapeutic activity of humanized anti-CD20 monoclonal antibody and polymorphism in IgG Fc receptor FcgammaRIIIa gene. Blood 99: 754–758.
19. Weng WK, Levy R (2003) Two immunoglobulin G fragment C receptor polymorphisms independently predict response to rituximab in patients with follicular lymphoma. J Clin Oncol 21: 3940–3947.
20. Miller AS, Tejada ML, Gazzano-Santoro H (2012) Development of an ELISA based bridging assay as a surrogate measure of ADCC. J Immunol Methods 385: 45–50.
21. Parekh BS, Berger E, Sibley S, Cahya S, Xiao L, et al. (2012) Development and validation of an antibody-dependent cell-mediated cytotoxicity-reporter gene assay. MAbs 4: 310–318.
22. Zhang W, Gordon M, Schultheis AM, Yang DY, Nagashima F, et al. (2007) FCGR2A and FCGR3A polymorphisms associated with clinical outcome of epidermal growth factor receptor expressing metastatic colorectal cancer patients treated with single-agent cetuximab. J Clin Oncol 25: 3712–3718.
23. Bruhns P, Iannascoli B, England P, Mancardi DA, Fernandez N, et al. (2009) Specificity and affinity of human Fcgamma receptors and their polymorphic variants for human IgG subclasses. Blood 113: 3716–3725.
24. Derer S, Glorius P, Schlaeth M, Lohse S, Klausz K, et al. (2014) Increasing FcγRIIa affinity of an FcγRIII-optimized anti-EGFR antibody restores neutrophil-mediated cytotoxicity. MAbs 6: 10–22.
25. Nagarajan S, Venkiteswaran K, Anderson M, Sayed U, Zhu C, et al. (2000) Cell-specific, activation-dependent regulation of neutrophil CD32A ligand-binding function. Blood 95: 1069–1077.
26. Tsuboi N, Asano K, Lauterbach M, Mayadas TN (2008) Human neutrophil Fcgamma receptors initiate and play specialized nonredundant roles in antibody-mediated inflammatory diseases. Immunity 28: 833–846.
27. Schneider-Merck T, Lammerts van Bueren JJ, Berger S, Rossen K, van Berkel PH, et al. (2010) Human IgG2 antibodies against epidermal growth factor receptor effectively trigger antibody-dependent cellular cytotoxicity but, in contrast to IgG1, only by cells of myeloid lineage. J Immunol 184: 512–520.
28. Tada M, Ishii-Watabe A, Maekawa K, Fukushima-Uesaka H, Kurose K, et al. (2012) Genetic polymorphisms of FCGR2A encoding Fcgamma receptor IIa in a Japanese population and functional analysis of the L273P variant. Immunogenetics 64: 869–877.
29. Suzuki T, Ishii-Watabe A, Tada M, Kobayashi T, Kanayasu-Toyoda T, et al. (2010) Importance of neonatal FcR in regulating the serum half-life of therapeutic proteins containing the Fc domain of human IgG1: a comparative study of the affinity of monoclonal antibodies and Fc-fusion proteins to human neonatal FcR. J Immunol 184: 1968–1976.
30. Heider KH, Kiefer K, Zenz T, Volden M, Stilgenbauer S, et al. (2011) A novel Fc-engineered monoclonal antibody to CD37 with enhanced ADCC and high proapoptotic activity for treatment of B-cell malignancies. Blood 118: 4159–4168.
31. Myszka DG (1999) Improving biosensor analysis. J Mol Recognit 12: 279–284.
32. Xu D, Alegre ML, Varga SS, Rothermel AL, Collins AM, et al. (2000) In vitro characterization of five humanized OKT3 effector function variant antibodies. Cell Immunol 200: 16–26.
33. Bertolotti-Ciarlet A, Wang W, Lownes R, Pristatsky P, Fang Y, et al. (2009) Impact of methionine oxidation on the binding of human IgG1 to Fc Rn and Fc gamma receptors. Mol Immunol 46: 1878–1882.
34. Pan H, Chen K, Chu L, Kinderman F, Apostol I, et al. (2009) Methionine oxidation in human IgG2 Fc decreases binding affinities to protein A and FcRn. Protein Sci 18: 424–433.
35. Wang W, Vlasak J, Li Y, Pristatsky P, Fang Y, et al. (2011) Impact of methionine oxidation in human IgG1 Fc on serum half-life of monoclonal antibodies. Mol Immunol 48: 860–866.
36. Bretaudeau L, Bonnaudet V (2011) ADCC potency assay: increased standardization with modified lymphocytes. BMC Proc 5 Suppl 8: P63.
37. Schnueriger A, Grau R, Sondermann P, Schreitmueller T, Marti S, et al. (2011) Development of a quantitative, cell-line based assay to measure ADCC activity mediated by therapeutic antibodies. Mol Immunol 48: 1512–1517.
38. Nelson DL, Kurman CC, Serbousek DE (2001) 51Cr release assay of antibody-dependent cell-mediated cytotoxicity (ADCC). Curr Protoc Immunol Chapter 7: Unit 7 27.
39. Carter PJ (2006) Potent antibody therapeutics by design. Nat Rev Immunol 6: 343–357.
40. Brennan FR, Morton LD, Spindeldreher S, Kiessling A, Allenspach R, et al. (2010) Safety and immunotoxicity assessment of immunomodulatory monoclonal antibodies. MAbs 2: 233–255.
41. Bugelski PJ, Achuthanandam R, Capocasale RJ, Treacy G, Bouman-Thio E (2009) Monoclonal antibody-induced cytokine-release syndrome. Expert Rev Clin Immunol 5: 499–521.
42. Wilde MI, Goa KL (1996) Muromonab CD3: a reappraisal of its pharmacology and use as prophylaxis of solid organ transplant rejection. Drugs 51: 865–894.
43. Suntharalingam G, Perry MR, Ward S, Brett SJ, Castello-Cortes A, et al. (2006) Cytokine storm in a phase 1 trial of the anti-CD28 monoclonal antibody TGN1412. N Engl J Med 355: 1018–1028.
44. Tax WJ, Tamboer WP, Jacobs CW, Frenken LA, Koene RA (1997) Role of polymorphic Fc receptor Fc gammaRIIa in cytokine release and adverse effects of murine IgG1 anti-CD3/T cell receptor antibody (WT31). Transplantation 63: 106–112.
45. Jonsson F, Mancardi DA, Zhao W, Kita Y, Iannascoli B, et al. (2012) Human FcgammaRIIA induces anaphylactic and allergic reactions. Blood 119: 2533–2544.
46. Kawakami T (2012) Human FcgammaRIIA at center stage. Blood 119: 2432–2433.
47. Cleland JL, Powell MF, Shire SJ (1993) The development of stable protein formulations: a close look at protein aggregation, deamidation, and oxidation. Crit Rev Ther Drug Carrier Syst 10: 307–377.
48. Vlasak J, Ionescu R (2008) Heterogeneity of monoclonal antibodies revealed by charge-sensitive methods. Curr Pharm Biotechnol 9: 468–481.
49. Liu D, Ren D, Huang H, Dankberg J, Rosenfeld R, et al. (2008) Structure and stability changes of human IgG1 Fc as a consequence of methionine oxidation. Biochemistry 47: 5088–5100.

8174–8187 Nucleic Acids Research, 2014, Vol. 42, No. 12 Published online 16 June 2014
doi: 10.1093/nar/gku512

Design and evaluation of locked nucleic acid-based splice-switching oligonucleotides *in vitro*

Takenori Shimo[1,†], Keisuke Tachibana[1,†], Kiwamu Saito[1], Tokuyuki Yoshida[1,2], Erisa Tomita[3], Reiko Waki[1], Tsuyoshi Yamamoto[1], Takefumi Doi[1], Takao Inoue[1,2], Junji Kawakami[3,4] and Satoshi Obika[1,*]

[1]Graduate School of Pharmaceutical Sciences, Osaka University, 1–6, Yamadaoka, Suita, Osaka, 565–0871, Japan, [2]Division of Cellular and Gene Therapy Products, National Institute of Health Sciences, 1–18–1 Kamiyoga, Setagaya-ku, Tokyo 158–8501, Japan, [3]Department of Nanobiochemistry, FIRST, Konan University, 7–1–20 Minatojima-minamimachi, Chuo-ku, Kobe 650–0047, Japan and [4]Frontier Institute for Biomolecular Engineering Research (FIBER), Konan University, 7–1–20 Minatojima-minamimachi, Chuo-ku, Kobe 650–0047, Japan

Received October 19, 2013; Revised May 22, 2014; Accepted May 23, 2014

ABSTRACT

Antisense-mediated modulation of pre-mRNA splicing is an attractive therapeutic strategy for genetic diseases. Currently, there are few examples of modulation of pre-mRNA splicing using locked nucleic acid (LNA) antisense oligonucleotides, and, in particular, no systematic study has addressed the optimal design of LNA-based splice-switching oligonucleotides (LNA SSOs). Here, we designed a series of LNA SSOs complementary to the human dystrophin exon 58 sequence and evaluated their ability to induce exon skipping *in vitro* using reverse transcription-polymerase chain reaction. We demonstrated that the number of LNAs in the SSO sequence and the melting temperature of the SSOs play important roles in inducing exon skipping and seem to be key factors for designing efficient LNA SSOs. LNA SSO length was an important determinant of activity: a 13-mer with six LNA modifications had the highest efficacy, and a 7-mer was the minimal length required to induce exon skipping. Evaluation of exon skipping activity using mismatched LNA/DNA mixmers revealed that 9-mer LNA SSO allowed a better mismatch discrimination. LNA SSOs also induced exon skipping of endogenous human dystrophin in primary human skeletal muscle cells. Taken together, our findings indicate that LNA SSOs are powerful tools for modulating pre-mRNA splicing.

INTRODUCTION

Alternative pre-mRNA splicing is an essential system for gene expression in eukaryotes that allows the production of various types of proteins from a limited set of genes (1). However, mutations in splice sites cause mis-splicing, which is followed by genetic diseases (2,3,4). To correct these splicing errors, exon skipping by using antisense oligonucleotides (AONs) has been suggested (5,6). These splice-switching oligonucleotides (SSOs) bind to target sequences in pre-mRNA and prevent the interaction of various splicing modulators (7). Thus, SSOs are able to modulate pre-mRNA splicing and repair defective RNA without inducing the RNase H-mediated cleavage of mRNA (8,9).

To enhance the *in vivo* activity of AONs, many artificial nucleic acids have been synthesized to improve nuclease resistance, binding properties, RNase H activity and serum stability (10,11). Locked nucleic acid (LNA) (also known as 2'-*O*,4'-*C*-methylene-bridged nucleic acid (2',4'-BNA)) is an artificial nucleic acid derivative that was synthesized by us and by Wengel's group independently in the late 1990s (12,13). LNA contains a methylene bridge connecting the 2'-*O* with the 4'-*C* position in the furanose ring, which enables it to form a strictly *N*-type conformation that offers high binding affinity against complementary RNA (14,15,16). LNA also presents enzyme resistance, similar to other nucleic acid derivatives. Given these features, LNA can be used for various gene silencing techniques, such as antisense, short interfering RNA, blocking of microRNA and triplex-forming oligonucleotides. Previous studies also showed that LNA could be used in SSOs (17,18,19,20), and LNA-based SSOs (LNA SSOs) have been shown to be functional *in vivo* in mouse models (21,22).

Recently, SSOs based on 2'-*O*-methyl RNA (2'-OMe) with a full-length phosphorothioate (PS) backbone,

*To whom correspondence should be addressed. Tel: +81 6 6879 8200; Fax: +81 6 6879 8204; Email: obika@phs.osaka-u.ac.jp
†The authors wish it to be known that, in their opinion, the first two authors should be regarded as Joint First Authors.

phosphorodiamidate morpholino oligomer or 2'-*O*,4'-*C*-ethylene-bridged nucleic acids have been applied to clinical trials for the treatment of genetic diseases, particularly Duchenne muscular dystrophy (DMD) (23,24,25,26,27,28). DMD is a severe muscle-weakening disease that arises from mutations in dystrophin, which links the cytoskeleton to the extracellular matrix of muscle fibers. Mutations in the dystrophin gene lead to premature termination of translation and prevent the synthesis of a functional gene product. SSO-mediated exon skipping in dystrophin pre-mRNA can restore the reading frame and allow the expression of a truncated but functional dystrophin similar to that found in Becker muscular dystrophy patients, who have relatively milder symptoms (29). Thus, modulation of splicing using SSOs is an attractive strategy for the treatment of genetic diseases, such as DMD. However, relatively few studies have used LNA SSOs compared to those using SSOs based on other chemistries.

Methods for designing effective SSOs have recently been developed and provide insight into factors that are critical for SSO activity, including the melting temperature (T_m), guanine-cytosine content and secondary structures or sequence motifs that correspond to splicing signals of the target RNA (30,31). Because LNA oligonucleotides possess high binding affinity to complementary RNA, the SSOs that incorporate LNA are considered as promising tools for inducing exon skipping. However, no systematic study has addressed the optimal design of LNA SSOs. Therefore, in this study, we designed a series of LNA SSOs complementary to the human dystrophin exon 58 sequence, and evaluated their ability to induce exon skipping using reverse transcription-polymerase chain reaction (RT-PCR) and a minigene reporter encompassing exons 57–59 of the human dystrophin gene.

MATERIALS AND METHODS

Synthesis of oligonucleotides

All SSOs used in this study are shown in Supplementary Tables S1–S9. Two types of modification, LNA and 2'-OMe, were incorporated into the SSO sequences, in which the phosphodiester linkages were completely replaced by PS linkages (Figure 1). All SSOs were designed to have sequences complementary to human dystrophin gene and were synthesized and purified by Gene Design Inc. (Osaka, Japan).

Plasmid construction

The reporter construct was generated using standard cloning techniques published in a previous study (32). A FLAG (DYKDDDDK)-coding oligonucleotide was constructed by annealing the forward oligonucleotide 5'-AGCTTACCATGGATTACAAGGACGACGAC GACAAGGGGGTAC-3' (including HindIII and KpnI sites, underlined) and reverse oligonucleotide 5'-CCCCTTGTCGTCGTCGTCCTTGTAATCCATGGTA-3'. The annealed oligonucleotide was cloned into the HindIII-KpnI sites of the pcDNA5/FRT vector (Invitrogen, Carlsbad, CA, USA) (termed pcDNA5/FRT-FLAG). The EGFP fragment was obtained by PCR using the forward primer 5'-CCCGGGTGTGAGCAAGGGCGAGGAGCTGT-3' (including a SmaI site, underlined) and reverse primer 5'-ATAGGGCCCTTACTTGTACAGCTCGTCCAT-3' (including an ApaI site, underlined). The obtained EGFP fragment was cloned into the EcoRV-ApaI sites of pcDNA5/FRT-FLAG (termed pcDNA5/FRT-FLAG-EGFP). The DsRed fragment was obtained by PCR from the pDsRed-Express-N1 vector (Clontech, Mountain View, CA, USA) using the forward primer 5'-ATATGGATCCAACCGGTGTGGCC TCCTCCGAGGACGTCA-3' (including BamHI and AgeI sites, underlined) and reverse primer 5'-CGGTCTACAGGAACAGGTGGTGGC-3'. The obtained DsRed fragment was cloned into the BamHI-SmaI sites of the pcDNA5/FRT-FLAG-EGFP vector (termed pcDNA5/FRT-FLAG-DsRed-EGFP). A nuclear localization signal (NLS) was constructed by annealing the forward oligonucleotide 5'-ATGCCCCAAAAAAAAA ACGCAAAGTGGAGGACCCAAAGGTACCAAAG-3' (including a KpnI site, underlined) and reverse oligonucleotide 5'-GATCCTTTGGTACCTTTGGGTCCTCCAC TTTGCGTTTTTTTTTTGGGGCATGTAC-3'. The annealing oligonucleotide was cloned into the KpnI-BamHI sites of pcDNA5/FRT-FLAG-DsRed-EGFP (termed pcDNA5/FRT-FLAG-NLS-DsRed-EGFP).

A human dystrophin minigene containing exons 57–59 was isolated as follows. Because the intron 57 sequence consists of 17 684 bp and is thus too long to insert into a plasmid, we designed a human dystrophin minigene by removing the sequence of intron 57 from position +207 to +17 486. Thus, exon 57, together with a short flanking intronic sequence, was obtained by PCR from the HepG2 genome using the forward primer 5'-AACGGTACCAACGCTGCTGTTCTTTTTCA-3' (including a KpnI site, underlined) and reverse primer 5'-GTGTTTGTAATGGACGATTTCTTAAAGGGTATT-3'. Another fragment containing a short 3' sequence of intron 57 to exon 59 was also obtained by PCR using the forward primer 5'-AAATCGTCCATTACAAACACAGCGCTTTCC-3' and reverse primer 5'-AGACCGGTACTCCTCAGCCTGCTTTCGTA-3' (including an AgeI site, underlined). These two fragments were mixed, and a second round of PCR was performed. Finally, after the second round of PCR, the newly synthesized full-length PCR product was cloned into the KpnI-AgeI sites of the pcDNA5/FRT-FLAG-NLS-DsRed-EGFP vector to generate a dystrophin reporter minigene (termed pcDNA5/FRT-FLAG-NLS-DMD-Exon57_58_59(short-Intron57)-DsRed-EGFP). All constructs were verified by sequencing.

Generation of a stable cell line

Flp-In 293 cells (Invitrogen) were cultured in Dulbecco's modified Eagle Medium (DMEM) (Nacalai Tesque, Kyoto, Japan) containing 10% fetal bovine serum (FBS) (Biowest, Nuaillé, France), 100 units/ml penicillin and 100 μg/ml streptomycin (Nacalai Tesque) and maintained in a 5% CO_2 incubator at 37°C. Flp-In 293 cells were

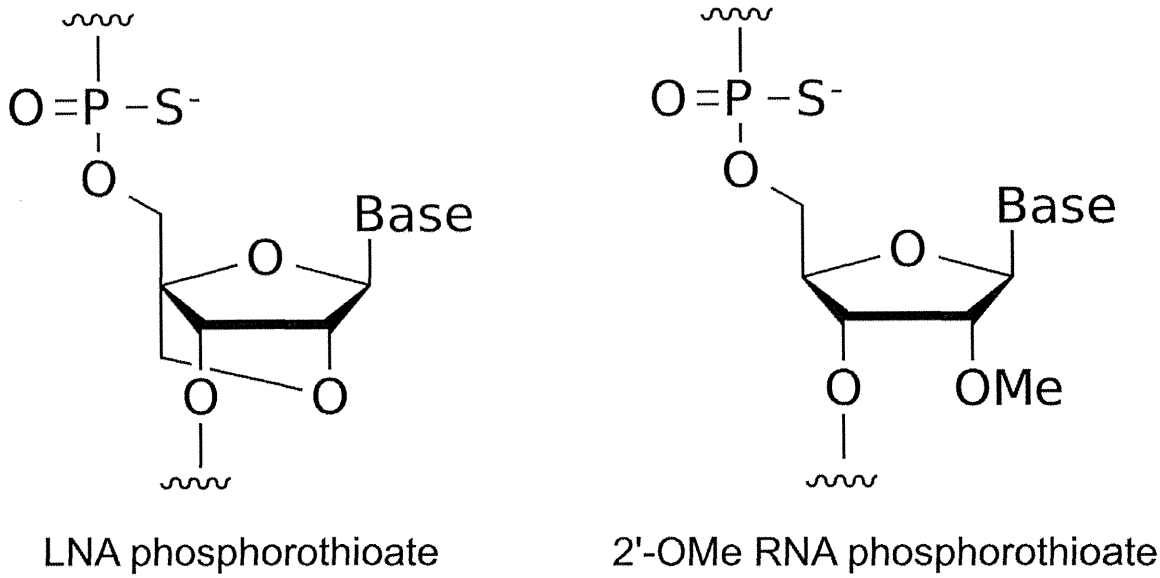

Figure 1. Structures of the building blocks for SSOs. PS LNA and PS 2'-OMe RNA.

co-transfected with pcDNA5/FRT-FLAG-NLS-DMD-Exon57_58_59(short-Intron57)-DsRed-EGFP and pOG44 (the flp recombinase expression plasmid) (Invitrogen). Stable cell lines were selected by 50 μg/ml hygromycin B (Invitrogen).

SSOs transfection

Stable cell lines were seeded one day before transfection at a density of 8.0×10^4 cells/well on 24-well plates. At 30%–40% confluence, SSOs were transfected into cells by using Lipofectamine 2000 (Invitrogen) according to the manufacturer's instructions. After 24 h, the cells were harvested.

RNA isolation and cDNA synthesis

Total RNA samples were isolated from the cells using the QuickGene 800 and QuickGene RNA cultured cell kit S (KURABO, Osaka, Japan) according to the manufacturer's instructions. First-strand cDNA was synthesized from 150 ng of the total RNA of each cell sample using the ReverTra Ace qPCR RT Master Mix (TOYOBO, Osaka, Japan) according to the manufacturer's instructions.

Primary myoblast cell culture, SSO transfection and RNA isolation

Primary human skeletal muscle myoblasts (HSMM) derived from healthy Caucasian donor (female aged 17 years) were purchased from Lonza (Walkersville, MD, USA). HSMM cells were cultured in SkBM-2 basal medium (Lonza) supplemented with 10% FBS, epidermal growth factor (EGF), dexamethasone, L-glutamine, gentamycin sulfate and amphotericin B (SingleQuots, Lonza) and maintained in a 5% CO_2 incubator at 37°C. For SSO transfection, cells were seeded 2 days before transfection at a density of 1.0×10^5 cells/well on 24-well collagen type I coated plates. After 24 h, cells were differentiated by changing the growth medium to differentiation medium (DMEM/F-12 (Life Technologies, Carlsbad, CA, USA) containing 2% horse serum (Life Technologies) and antibiotic-antimycotic solution (100 units/ml penicillin, 100 μg/ml streptomycin, 0.25 μg/ml amphotericin B) (Life Technologies)) for 24 h. Cells were transfected with 500 nM SSOs using Lipofectamine 2000 according to the manufacturer's instructions. Twenty-four hours after transfection, total RNA samples were isolated from the cells using the QuickGene 800 and QuickGene RNA cultured cell kit S according to the manufacturer's instructions. First-strand cDNA was synthesized from 50 ng of the total RNA of each cell sample using the ReverTra Ace qPCR RT Master Mix according to the manufacturer's instructions.

RT-PCR analysis

The cDNA was used as a template for individual PCR reactions using specific primer sets (Supplementary Table S10), which were designed using the Primer3 program written by the Whitehead Institute (33). PCR reactions were conducted using KOD FX Neo DNA polymerase (TOYOBO), and the PCR products were analyzed on a 2% agarose gel stained with ethidium bromide, with specific bands purified for sequence analysis. The intensity of each band was quantified by using ImageJ software (National Institutes of Health; freeware from http://rsb.info.nih.gov/ij/) and normalized according to the nucleotide composition. The exon skipping percentage was calculated as the amount of exon 58-skipped transcript relative to the total amount of the exon 58-skipped and full-length transcripts (34). Glyceraldehyde-3-phosphate dehydrogenase (GAPDH) was used as an internal control.

Quantitative real-time RT-PCR analysis

The cDNA was used as a template for individual PCR reactions using exon skipping specific primer sets (Supplementary Table S11), which were designed using the Primer Express program (Applied Biosystems, Foster City, CA, USA) and Primer3 program. PCR reactions were conducted using SYBRGreen Real-time PCR Master Mix (TOYOBO) according to the manufacturer's instructions, except that the annealing time was reduced to 15 s. The quantitative PCR analysis was performed using the StepOnePlus device (Applied Biosystems). Amplification specificity was verified by visualizing the PCR products on an ethidium bromide-stained 2% agarose gel. GAPDH was used to normalize the expression data.

Ultraviolet (UV) melting experiment

UV melting experiments were conducted using a Shimadzu UV-1650PC UV-Vis spectrophotometer equipped with a T_m analysis accessory TMSPC-8 (Shimadzu, Kyoto, Japan). Equimolecular amounts of SSO and complementary RNA oligonucleotide were dissolved in 10 mM sodium phosphate buffer (pH 7.2) containing 10 mM NaCl to give a final strand concentration of 2.0 μM. The samples were boiled for 3 min, followed by slow cooling to room temperature. The absorption was recorded at 260 nm in the forward and reverse direction from 5°C to 95°C at a scan rate of 0.5°C/min. The first derivative was calculated from the smoothed UV melting profile. The peak temperatures in the derivative curve were designated as the melting temperature, T_m.

In silico analysis to search for target sequence

To know the number of genes that contain the sequence perfectly matched to the target sequence of AONs, we used GGRNA, a Google-like fast search engine for genes and transcripts (http://GGRNA.dbcls.jp/) (35). In this analysis, we considered splicing variants with the same gene ID as one gene and excluded the genes which do not encode proteins.

RESULTS

Screening for LNA SSOs effective for inducing exon skipping

We performed a screening analysis to obtain effective LNA SSOs that induced skipping of exon 58 of the human dystrophin gene. Prior to starting the screening of the SSOs, we developed a minigene reporter plasmid containing exons 57–59 of the human dystrophin gene. Subsequently, we established a stable reporter cell line in which the reporter plasmid was incorporated into the genomic DNA and used as a splicing assay system. To evaluate the efficacy of the designed SSOs, the reporter cells were transfected with each SSO, and exon skipping was analyzed by RT-PCR (Supplementary Figure S1).

In this screening study, we designed a series of 15-mer LNA/DNA mixmers with a LNA substitution at every third nucleotide position. These mixmers contained five LNA units in the SSO sequence, in which the phosphodiester linkages were completely replaced by PS linkages (Figure 1). To prevent RNase H-dependent RNA degradation, we designed the number of continuous natural nucleotides in the SSO to be less than two (Figure 2A) (36). The screening was composed of three steps. At the first step, nine non-overlapping LNA SSOs were designed to tile across the entire target exon 58 sequence to detect a prospective target site (Figure 2B and Supplementary Table S1). Reporter cells were transfected with 100 nM SSOs for 24 h. Total RNA samples were prepared, and RT-PCR analyses showed that three LNA SSOs, i.e. -5+10, +70+84 and +115-8, were effective in slightly inducing exon skipping of exon 58 (the rate of exon skipping was 10%–20%) (Figure 2C and Supplementary Figure S2A).

In the second step, to detect the more active SSOs, we synthesized three sets of 15-mer LNA SSOs shifted by three bases around each expected target sequence, i.e. -5+10, +70+84 and +115-8 (Figure 2D and Supplementary Table S2). These SSOs (100 nM) were transfected into the reporter cell line, and total RNA samples were prepared after a further 24 h incubation. The RT-PCR results suggested that both the 5′ and 3′ splice sites in addition to the 27-base region from +70 to +96 of exon 58 are hot spots for inducing exon skipping (Figure 2E and Supplementary Figure S2B). In addition, this region was predicted as an exonic splicing enhance (ESE) site by ESEfinder3.0 (Supplementary Figure S3) (37,38). In this case, we decided to select two SSOs, -2+13 and +106+120, as templates for the next screening step given their high ability to modulate splicing (the rate of exon skipping increased to ca. 50%) (Supplementary Figure S2B).

Finally, we designed a further four LNA SSOs shifted by one nucleotide around each SSO, i.e. -2+13 and +106+120 (Figure 2F and Supplementary Table S3). In the third step, we assessed the expression of exon 58-skipped mRNA by means of quantitative real-time RT-PCR to rigorously evaluate the abilities of the SSOs. Both the SSO (-1+14) in the 5′ splice site and the SSO (+108-1) in the 3′ splice site showed higher exon 58 skipping activity (Figure 2G). Surprisingly, in some cases SSOs that are frameshifted by one nucleotide resulted in loss of SSO activity (e.g. -4+11 versus -3+12). These findings demonstrate that exon 58 skipping can be modulated by 15-mer LNA/DNA mixmer SSOs targeting near the 5′ and 3′-splice sites of exon 58, and that this activity is strongly dependent on the target sequence.

Evaluation of the effect of number of LNAs and T_m value on splicing

In the following experiments, we selected two sequences identified from the above screening for exon skipping (-1+14 and +108-1). To investigate the relationship between the number of LNAs in the sequence of the SSOs and skipping activity, we synthesized a series of 15-mer SSOs that had various numbers of LNAs (Figure 3A). To protect the SSOs against nuclease degradation and prevent RNase H-induced pre-mRNA digestion, 2′-OMe RNAs were introduced into SSOs if fewer than five LNAs were in the sequence. We determined the T_m values of these SSOs with complementary RNA by UV melting experiments per-

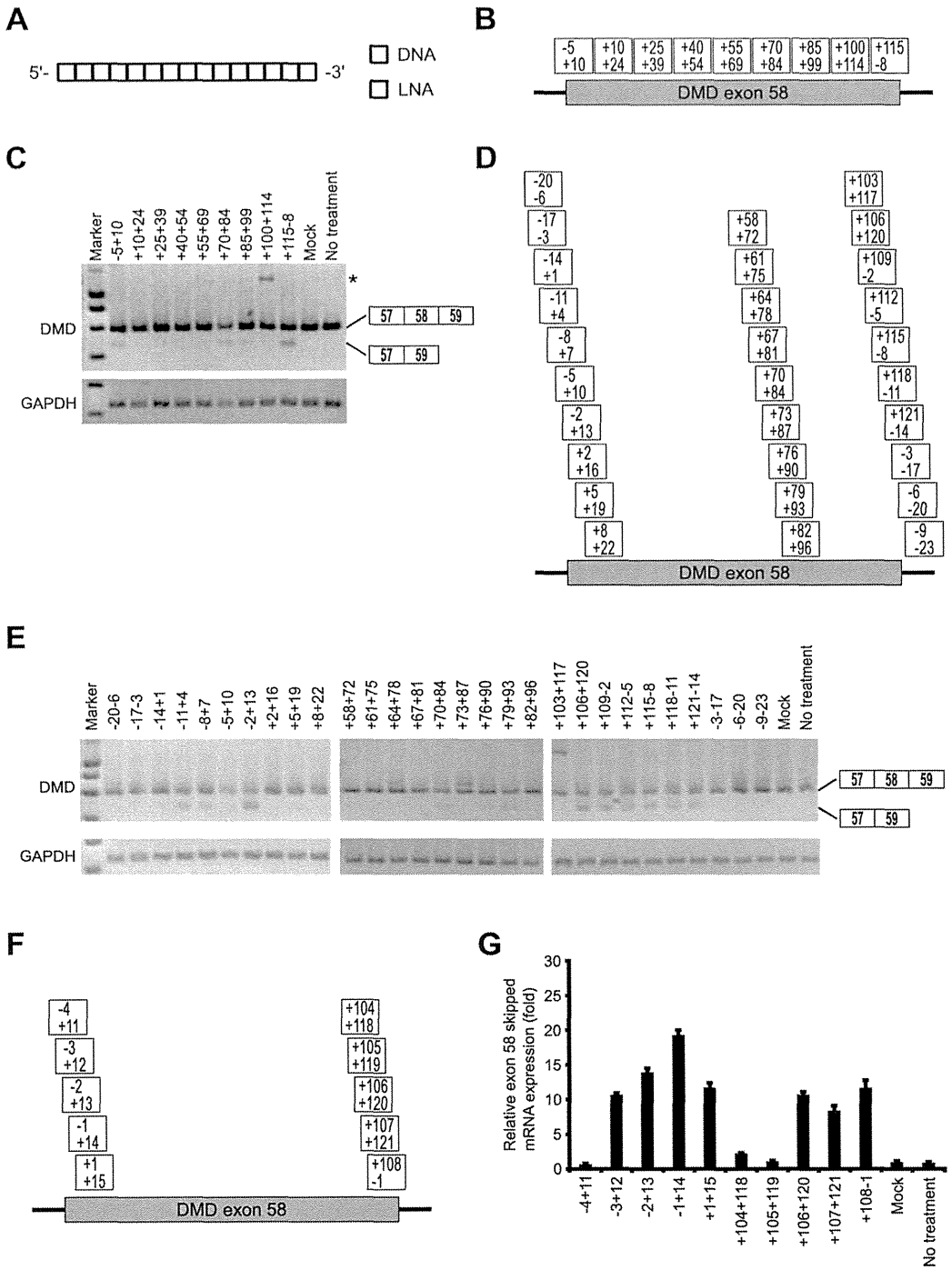

Figure 2. Screening of 15-mer LNA/DNA mixmer SSOs designed to induce dystrophin exon 58 skipping. (**A**) Schematic representation of the position of LNA in the 15-mer SSO used in this screening. Each box represents one nucleotide; the blue box and yellow box indicate LNA and DNA, respectively. (**B, D, F**) Annealing sites of SSOs targeted to dystrophin exon 58 are indicated by the boxes for the first (B), second (D) and third screening (F). (**C, E**) The reporter cells were transfected with the indicated LNA/DNA mixmer SSOs (100 nM) for 24 h. RT-PCR analyses showing the full-length upper band (587 bp) and the skipped lower band (466 bp). The band marked by an asterisk represents an intron 58 inclusion product. GAPDH was used as an internal control. (C) and (E) express the results of the first and second screening, respectively. (**G**) The levels of exon 58-skipped mRNA fragments were measured by quantitative real-time RT-PCR and normalized against the signal of GAPDH mRNA, relative to the value in the mock set as 1. Values represent the mean ± standard deviation of triplicate samples. Reproducible results were obtained from two independent experiments. Mock: treated with Lipofectamine only; no treatment: no transfection.

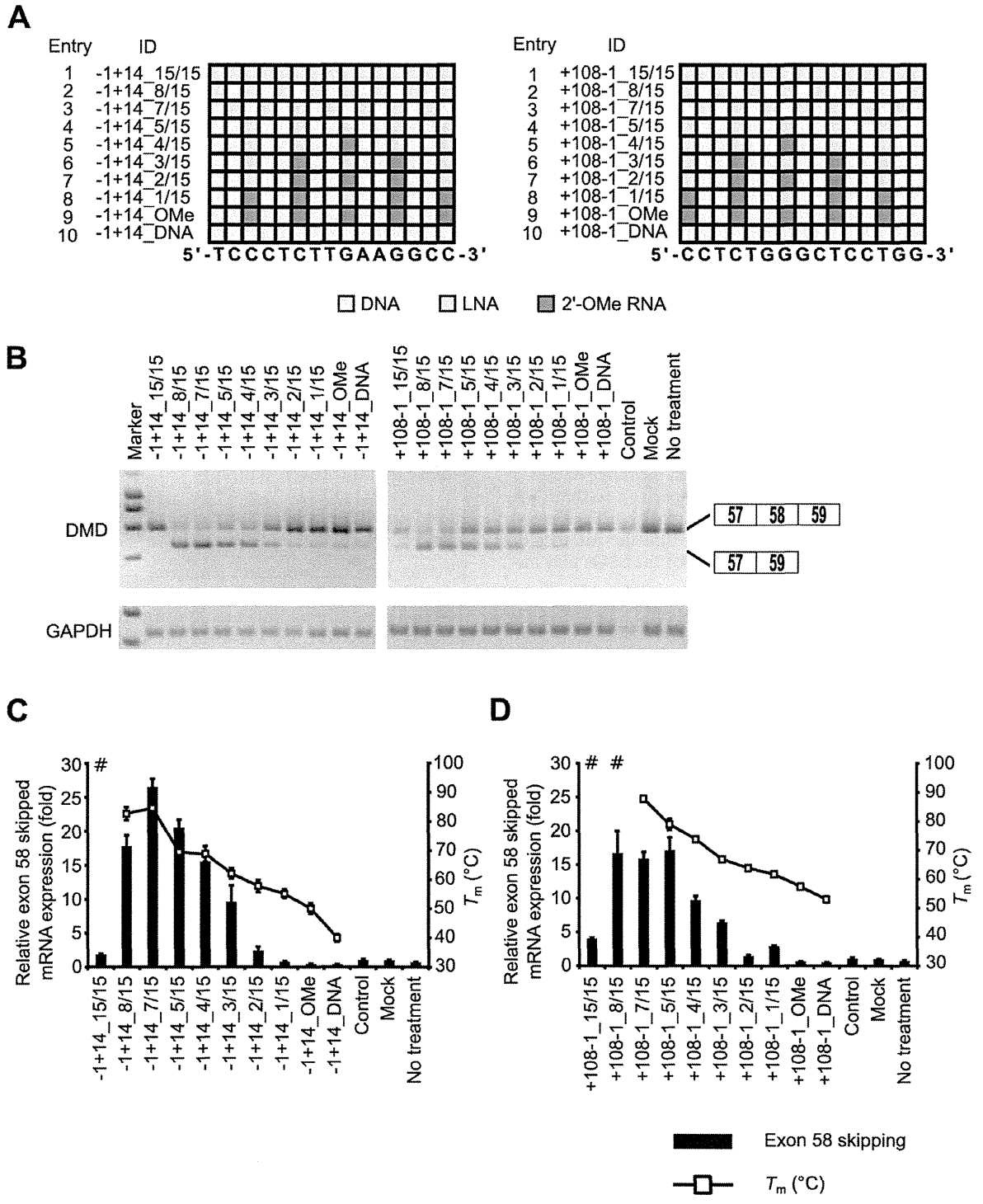

Figure 3. Evaluation of exon skipping activity of 15-mer SSOs with various numbers of LNAs and T_m values. (**A**) Schematic representation of the position of LNA in the 15-mer SSOs used in this study. Each box represents one nucleotide; the blue box, red box and yellow box indicate LNA, 2′-OMe RNA and DNA, respectively. (**B**) The reporter cells were transfected with the indicated LNA/DNA mixmer SSOs (30 nM) for 24 h. RT-PCR analyses were performed as described in Figure 2C. LNA SSO (+10+24), which showed no exon skipping effects, was used as a control. (**C** and **D**) The levels of exon 58-skipped mRNA fragments were measured by quantitative real-time RT-PCR (for details see Materials and Methods and Figure 2G). Values represent the mean ± standard deviation of triplicate samples. Reproducible results were obtained from two independent experiments. The T_m of each SSO with a complementary RNA under low-sodium conditions is also shown. # indicates that no sigmoidal melting curve was observed, even at higher T_m values. The data are the mean ± standard deviation ($n = 4$). (C) and (D) express exon skipping results of using SSOs targeted the 5′ and 3′ splice sites, respectively.

formed under low-sodium conditions (10 mM phosphate buffer (pH 7.2) containing 10 mM NaCl) (Supplementary Tables S4 and S5). The lower ionic concentration of the solvent tended to decrease T_m relative to the typical ionic concentrations, such as 100 mM NaCl (Supplementary Table S4). LNA SSO (+10+24) did not show an exon skipping effect (Figure 2C) and was thus used as a control.

We transfected reporter cells with 30 nM SSOs, and the cells were then incubated for 24 h. Then, total RNA samples were prepared, and exon 58-skipped mRNA levels were determined by both RT-PCR and quantitative real-time RT-PCR. RT-PCR analysis indicated that increasing the number of LNAs enhanced exon skipping activity (the rate of exon skipping reached 80%) (Figure 3B and Supplementary Figure S4A and B). Similar results were obtained by quantitative real-time RT-PCR assays, and SSOs containing between five and eight LNAs induced exon skipping at high levels (Figure 3C and D). On the other hand, SSOs fully modified with LNA showed very low activity, and their T_m values were higher than 95°C. In our experiments, efficient exon skipping activity was obtained when LNA/DNA mixmer SSOs were designed with a T_m in the range of 60°C–90°C (low sodium conditions). In comparison to the LNA SSOs, both the 2′-OMe SSO and DNA SSO hardly affected exon skipping. These results indicate that the number of LNA in the SSO sequence and the T_m of the SSOs play important roles in exon skipping.

Influence of SSO length on exon skipping

To determine whether the SSO length affects splicing modulation, we tested SSOs targeting the 3′ splice site. The length of the SSOs ranged from 9 to 23 nucleotides. Taking into account the T_m values of the short SSOs, we designed eight SSOs that contained 50% LNAs in their sequences (Figure 4A and Supplementary Table S6). We also determined dissociation constant (K_d) for LNA/DNA mixmer SSOs to mRNA (Supplementary Materials and Methods and Supplementary Table S6).

Reporter cells were transfected with 30 nM SSOs. Total RNA samples were prepared after a further 24 h incubation, and we assessed the expression of exon 58-skipped mRNA by means of RT-PCR and quantitative real-time RT-PCR. RT-PCR revealed that the longer LNA SSOs induced exon skipping with high efficiency (the rate of exon skipping was ~75%) (Figure 4B and Supplementary Figure S5). Intriguingly, when the levels of exon 58-skipped mRNA were analyzed by quantitative real-time RT-PCR, the 13-mer SSO (+110-1_6/13) produced high amounts of exon 58 skipping mRNAs in a concentration-dependent manner (Figure 4C–E and Supplementary Figure S6A). A concentration-dependent increase was also observed for other SSO (-1+14_7/15) targeting the 5′ splice site (Supplementary Figure S6B–D). Amazingly, the 9-mer LNA SSO (+114-1_4/9) (T_m = 66.7°C) induced exon skipping, in a similar manner as 19-, 21- and 23-mer SSOs (Figure 4C).

Characterization of 9-mer LNA SSOs

Although no reports to date have indicated that 9-mer SSOs induce exon skipping, we found that even a 9-mer SSO (+114-1_4/9) (four LNA and five DNA) could modulate splicing, albeit weakly. Therefore, to further improve the efficiency of exon skipping, we designed another two 9-mer SSOs containing seven LNAs having the same sequence as +114-1_4/9 (Figure 5A and Supplementary Table S7). As expected, the T_m values of both SSOs (+114-1_7/9_1 and +114-1_7/9_2) were higher than that of SSO (+114-1_4/9) (87.1°C, 83.1°C, and 66.7°C, respectively) (Supplementary Table S7).

The reporter cells were treated with 30 nM SSOs for 24 h and then subsequently lysed with the total RNA extracted. Interestingly, 9-mer LNA SSO (+114-1_7/9_2) presented 1.5-fold higher activity than the other 9-mer LNA SSOs (Figure 5B and C and Supplementary Figure S7). It seems that the position of LNA analogues in the SSO sequence may be a key factor for exon skipping. Moreover, this 9-mer SSO induced exon skipping in a concentration-dependent manner (Figure 5D and Supplementary Figure S8A–E). In contrast, the 9-mer 2′-OMe SSO (T_m = 40.0°C) exhibited no exon skipping activity at all. In this study, we report for the first time that 9-mer LNA SSOs have sufficient activity to induce exon skipping.

Short 7-mer LNA SSO-induced exon skipping in the reporter cells

To determine the minimum length of LNA SSO required for inducing exon skipping, we tested short LNA SSOs (6- to 9-mer) containing various numbers of LNAs (Supplementary Table S8). We designed three sets of LNA SSOs (fully modified LNA SSOs which have as high T_m value as possible, LNA/DNA mixmer SSOs containing 50% LNAs, such as Figure 4A, and LNA/DNA mixmer SSOs containing two DNAs like a +114-1_7/9_2, respectively) for each length (Figure 6A).

Reporter cells were transfected with 30 nM SSOs. Total RNA samples were prepared after a further 24 h incubation, and we assessed the expression of exon 58-skipped mRNA by means of RT-PCR and quantitative real-time RT-PCR. RT-PCR revealed that 9-, 8- and 7-mer LNA SSOs induced exon skipping, while 6-mer LNA SSOs did not show any activity (Figure 6B and Supplementary Figure S9). In the case of short LNA SSOs, the longer SSOs tend to have higher activity and exon skipping activity was obtained when LNA SSOs were designed with a T_m higher than 60°C (low sodium conditions) (Figure 6C). These results indicate that even very short 7-mer LNA SSO provides exon skipping activity.

Effect of mismatches on exon skipping activity and sequence specificity

To assess the specificity of LNA SSOs, we introduced one, two or three mismatches in both 13- and 9-mer LNA SSOs (Figure 7A and B and Supplementary Table S9). The reporter cells were transfected with 30 nM LNA SSOs. Twenty-four hours after transfection, total RNAs were extracted and the expression levels of exon 58-skipped mRNA were analyzed by both RT-PCR and quantitative real-time RT-PCR (Figure 7C and D and Supplementary Figure S10). We observed that when one LNA mismatch is introduced into 13-mer LNA SSO (six LNA and seven DNA)